Contents

1 Refinements and Additions to EOI

1.1 Measuring the B_s mixing parameter x_s

In section 4.2 of the BTeV EOI a discussion of the x_s reach of the BTeV detector was presented using the decay $B_s \to \psi \overline{K}^{*0}$. Since the EOI, this work has been improved both by extending the analysis and by the inclusion of a new mode, $B_s^0 \to D_s^- \pi^+$, $D_s^- \to \phi \pi^-$, $\phi \to K^+ K^-$.

The topology of this mode differs from $\psi \overline{K}^{*0}$ where all four tracks come from the B_s decay vertex. Here we use the information that a) the D_s^- candidate forms a 3-prong vertex which is well separated from the main vertex; b) the D_s^- trajectory intersects that of the π^+ to form a 2-prong vertex which is also well separated from the main vertex; c) the $D_s^- \pi^+$ combination has a momentum vector which points back at the main vertex.

In the first step of this analysis, pairs of oppositely charged tracks were selected, with the requirements that each track lie in the momentum range between 3 and 70 GeV/c and that each be identified as a kaon by the RICH system. Pairs which passed these cuts were retained as ϕ candidates provided the invariant mass of the pair lay within 20 MeV/c^2 of the ϕ mass ($\sigma \approx 5$ Mev/c^2). In the following steps, any track not identified by the RICH as a kaon was accepted as a $\pi^\pm$ candidate. The ϕ candidates were then combined with each remaining $\pi^\pm$ candidate in the event. The three track system was retained as a $D_s^\pm$ candidate provided its invariant mass was within 25 MeV/c^2 of the D_s mass ($\sigma \approx 5$ Mev/c^2) and provided the candidate passed a vertex constrained fit with a $\chi^2 < 10$. Finally, each $D_s^\pm$ was combined with each $\pi^\mp$ candidate and the combination was retained as a B_s candidate provided its mass lay within ± 50 MeV/c^2 of the B_s mass ($\sigma \approx 14$ Mev/c^2) and provided it passed a constrained vertex fit with a $\chi^2 < 6$. As with the $\psi \overline{K}^{*0}$ analysis, the primary vertex pattern recognition and fitting was redone for each $D_s^\pm \pi^\mp$ combination. The following cuts were then applied; each track must have at least 3 hits in the pixel detector; each track must have an impact parameter with respect to the primary vertex of more than 3σ; both vertices were required to have significant detachments, $L/\sigma_L(D_s) > 4.0$ and $L/\sigma_L(B_s) > 4.0$. Finally, the B_s candidate was required to point back to the primary vertex. The model of the trigger used in this analysis was 2 tracks, each with $p_y > 0.5$ GeV/c and each with an impact parameter of more than 4 σ. After all cuts it was found that about 2400 events/year will be triggered, reconstructed and tagged. See Table 1 for a breakdown of the contributions to this number. Finally, this mode achieved a mean resolution on the proper decay time of the B_s of approximately 52 fs.

It is anticipated that the dominant background to this mode will be $B \to D_s X$ events, where B includes all species of B hadrons which can decay to D_s. An MCFast study of this background source showed that the expected signal to background level in this mode is approximately 3:1.

It now appears that the $D_s^\pm \pi^\mp$ mode will have a greater x_s reach than will the $\psi \overline{K}^{*0}$ mode. Both modes have similar signal to background levels, while the statistics strongly favor the former and the time resolution only slightly favors the latter. However, the $\psi \overline{K}^{*0}$ mode remains of interest because it can be triggered both by the secondary vertex trigger and by various muon based triggers.

Fig. 1 shows the unmixed (a) and mixed (b) B_s decay proper time distributions generated with an x_s equal to 40 for the $D_s^\pm \pi^\mp$ mode. These figures were generated using the mini Monte Carlo described in the EOI, but with the "box" smearing function replaced by a Gaussian smearing function. This is particularly important when the experiment is limited by time resolution, not by statistics. Fig. 1(c) shows the negative Log Likelihood function computed from the Monte Carlo events in (a) and (b). The fit correctly picks out the proper solution at $x_s = 40$.

The $n\,\sigma$ error contours are defined by a step of $0.5n^2$ units of likelihood above the minimum. The mini Monte Carlo predicts an uncertainty in x_s of ± 0.1 for one year of running at $\mathcal{L} = 5 \times 10^{31} \mathrm{cm}^{-2} \mathrm{s}^{-1}$. Also, one can define a significant observation as one in which the deepest minimum is deeper than the next deepest minimum by at least "5 σ", that is by 12.5 units of likelihood. This level above the minimum is shown by the dashed line.

We also improved and corrected the $B_s \to \psi \overline{K}^{*0}$ analysis. In the EOI the only source of background to be extensively studied was combinatoric background within signal events. It is expected that the most important source of background will be events of the form $B \to \psi X$, $\psi \to \mu^+ \mu^-$, where B denotes any B hadron species which may decay to ψ. This background was studied using an MCFast simulation of approximately 500,000 such events, which showed that a signal to background ratio of 3.0 ± 0.6 could be

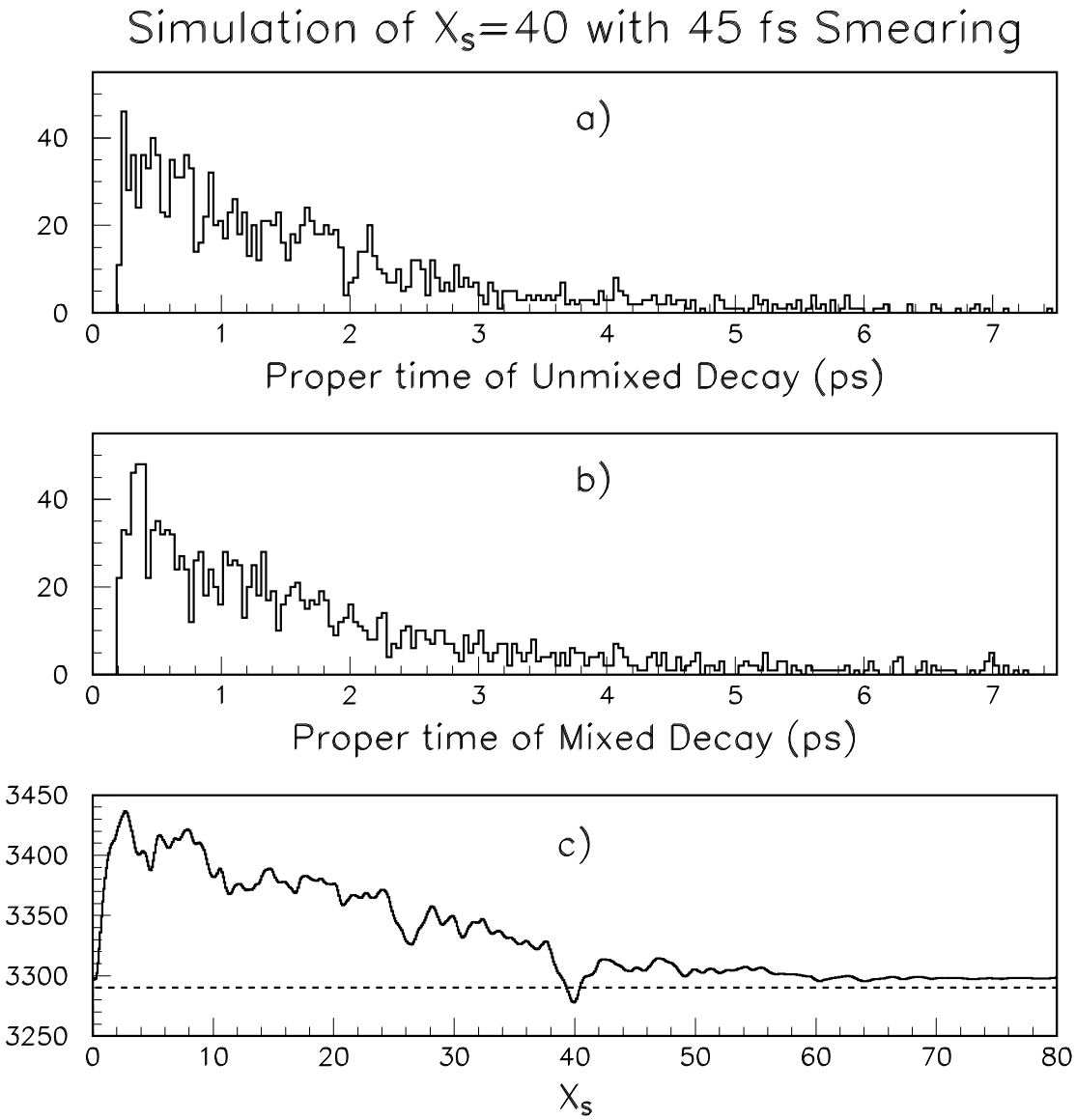

Figure 1: Mini Monte Carlo results for measuring x_s using $B_s \rightarrow D_s^{\pm}\pi^{\mp}$ in one year of BTeV running at $\mathcal{L} = 5 \times 10^{31}\mathrm{cm}^{-2}\mathrm{s}^{-}1$; a) Proper decay time distribution for unmixed decays; b) Proper decay time distribution for mixed decays; c) Negative Log Likelihood function computed from the entries in parts a) and b). The dashed line across part c) shows the level which is 5 σ above the minimum.

achieved using the same cuts as were designed to remove combinatoric background from within signal events. In order to obtain adequate statistics for the background study, it was necessary to count events in a broad sideband region about the signal region. The quoted error in the signal to background ratio reflects the uncertainty in the shape of the background mass distribution. This background level was deemed acceptable and this level of background was added to the mini Monte Carlo simulation. Also, an error was found in the estimate of the mistag fraction, which is 0.25, not 0.15 as stated in the EOI.

Another improvement to the x_s analysis was in understanding how to make a systematic statement about the x_s reach of the detector. The shape of the likelihood function, without the statistical fluctuations, can easily be calculated analytically following McDonald [8]. Fig. 2 shows this likelihood function for the same inputs as used for Fig. 1. One can see that the two figures have the same basic shape but that the later has no statistical fluctuations. In this case there are no secondary minima so one can define a significant observation as one in which the minimum is at least 12.5 units of likelihood deeper than the asymptotic value of the likelihood function. While this this definition allows signals which are slightly less significant than does the definition above it is a practical alternative for this case.

The critical observation is that, if the number of events in the sample is changed, then the shape of the likelihood function does not change, rather it simply scales proportionally to the number of events. This can be stated formally as follows. Let x_0 denote the generated value of x_s and let $\mathcal{L}(x; x_0, N)$ denote the value of the likelihood function, evaluated at x, for a sample which has a true value of x_0 and which contains N events. Then,

$$\mathcal{L}(x; x_0, N) \quad = \quad N\mathcal{L}(x; x_0, 1) \tag{1}$$

Now, one can define the significance of the minimum, n, as,

$$n^2 \quad = \quad 2.0N\left[\mathcal{L}(\infty; x_0, 1) - \mathcal{L}(x_0; x_0, 1)\right]. \tag{2}$$

For practical purposes ∞ was chosen to be 160 and the definition of a significant signal was that $n = 5$. Finally, the last equation was solved for N, which is easily converted into a running time. The solid line in Fig. 3 shows the number of years needed to obtain a significant measurement as a function of x_s. For reference, the same information is shown for the $\psi\overline{K}^{*0}$ final state as the dotted curve in that figure.

Finally, a proposed new pixel detector layout with a square hole, described in section 1.4.4, has been shown to dramatically improve both the time resolution and the acceptance for both of the modes being studied. The main design change is to fill in the vertical gap with pixels, leaving only a square hole 1.2 cm on a side for the beams to pass through. For the mode $\psi\overline{K}^{*0}$, the acceptance increases by 70% while the mean time resolution drops from 45 fs to 33 fs. The x_s reach of this modified detector is shown as the dot-dashed line in Fig. 3. For the mode $D_s^{\pm}\pi^{\mp}$, the acceptance increases by 50% while the mean time resolution drops from 52 fs to 38 fs. The increased x_s reach in this mode is shown as the dashed line in Fig. 3. Clearly $x_s = 40$ is within the one year reach of the EOI detector at $\mathcal{L} = 5 \times 10^{31}\text{cm}^{-2}\text{s}^{-1}$ and of $x = 60$ is within the one year reach of the square-hole detector $\mathcal{L} = 5 \times 10^{31}\text{cm}^{-2}\text{s}^{-1}$.

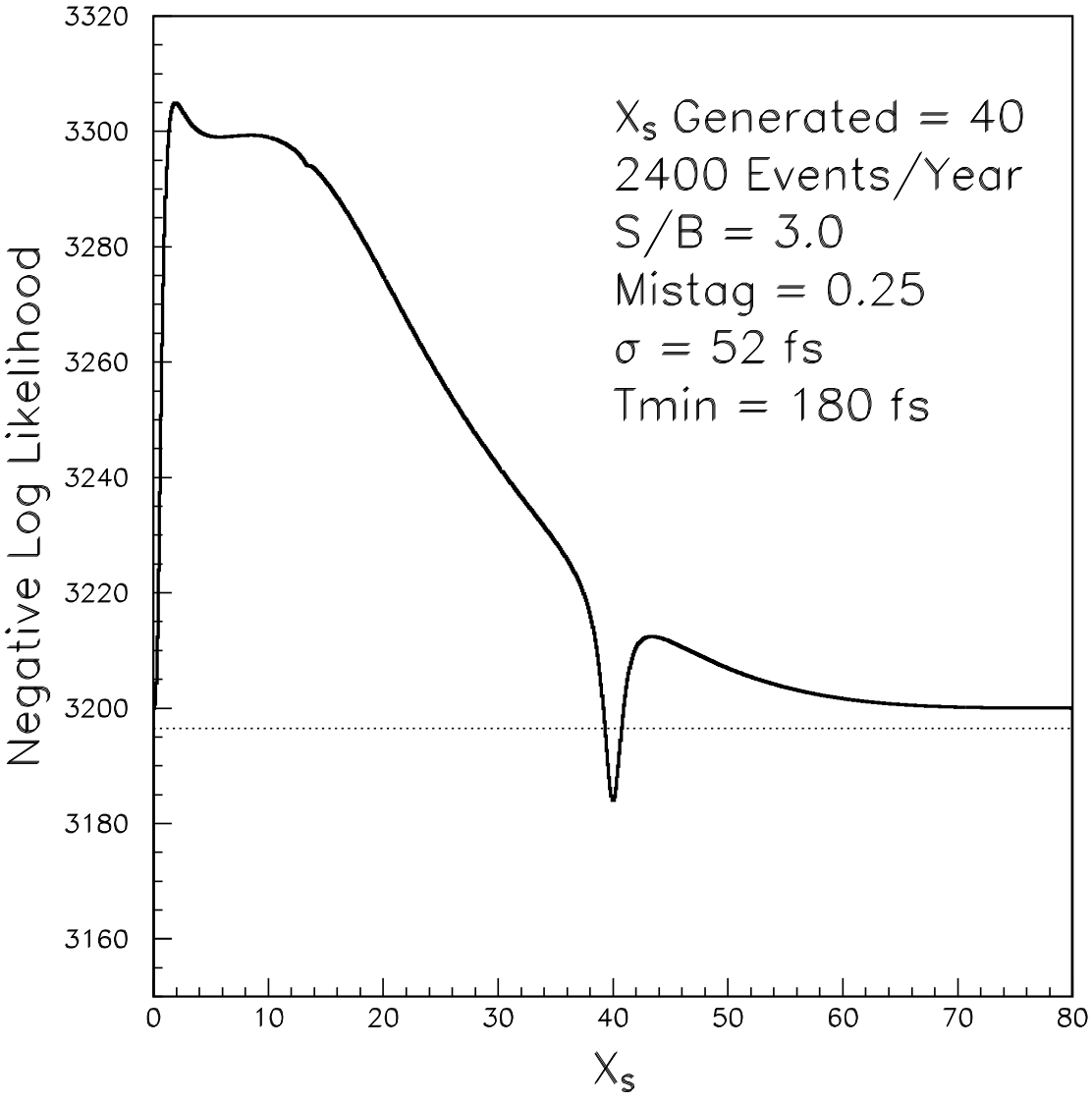

Figure 2: Negative Log Likelihood function calculated analytically as described in the text for the same conditions as for Fig. 1. The overall shape is the same but the statistical fluctuations are removed.

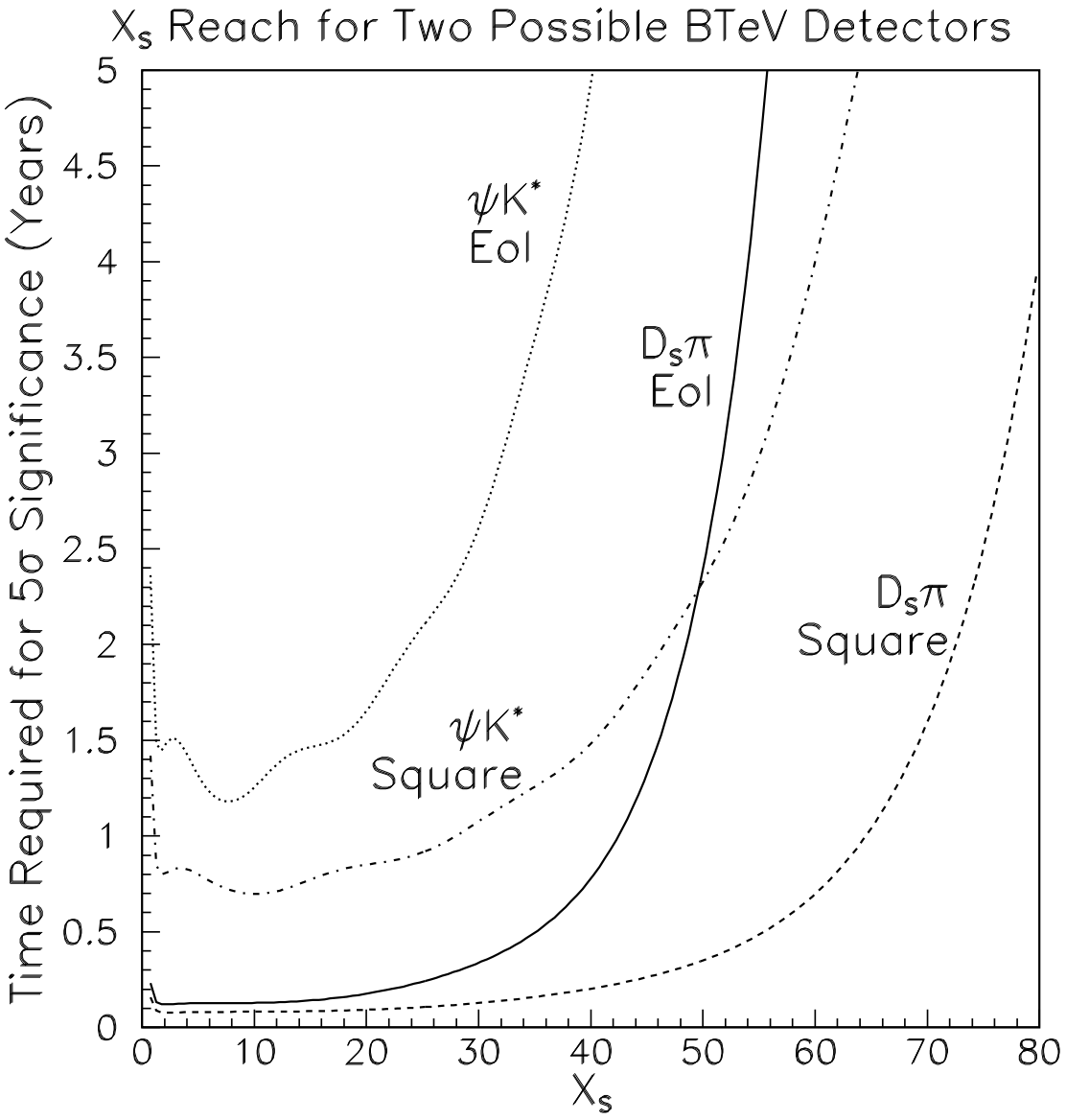

Figure 3: The x_s reach of the BTeV detector using the mode $B_s \to D_s^{\pm}\pi^{\mp}$. The solid curve indicates, for a given value of x_s, the number of years of running the EOI detector at $\mathcal{L} = 5 \times 10^{31}\mathrm{cm}^{-2}\mathrm{s}^{-1}$ which are required to obtain a 5σ measurement. The dotted curve indicates the same information but for the $\psi\overline{K}^{*0}$ final state. The other two lines show the improvement in reach obtained by using the square-hole detector proposed in section 1.4.4; the dashed curve is for $B_s \to D_s^{\pm}\pi^{\mp}$ and the dot-dashed curve is for $\psi\overline{K}^{*0}$.

Luminosity	5×10^{31}
Running time	10^7 sec
Integrated Luminosity	500 pb-1
$\sigma_{b\bar{b}}$	100μb
Number of $B\overline{B}$ events	5×10^{10}
Number of $B_s^0 + \overline{B}_s^0$	1.3×10^{10}
B$(B_s^0 \to D_s^- \pi^+)$	3.0×10^{-3}
B$(D_s \to \phi\pi^+) \times \mathcal{B}(\phi \to K^+K^-)$	1.8×10^{-2}
Reconstruction efficiency	0.033
Trigger efficiency	0.70
Number of reconstructed $B_s^0(\overline{B}_s^0) \to D_s K$	16,000
Tagging efficiency ϵ	0.15
Number of tagged events	2400
Mistag Fraction	0.25

Table 1: Projected Yield for $B_s \to D_s^{\pm}\pi^{\mp}$ in one year of BTeV running. The trigger efficiency is quoted as a fraction of those events which pass the reconstruction. The tagging efficiency and mistag fraction are quoted from the sum of the clean tagging modes only.

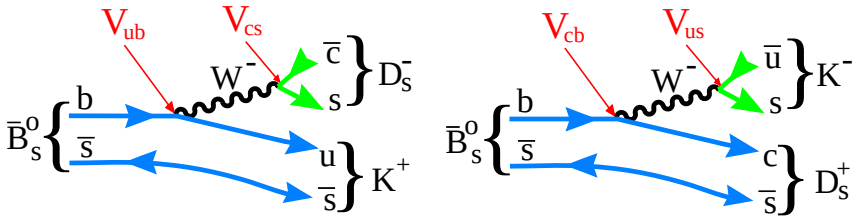

Figure 4: Two diagrams for $\overline{B}_s^o \to D_s^{\pm} K^{\mp}$ showing the relevant CKM matrix elements.

1.2 Measuring γ

There have been several suggestions on how to measure the CKM angle γ. Two of them appear to have potential experimental difficulties, while one may have theoretical ambiguities. We give a status report here of our simulations of these three methods.

1.2.1 $B_s \to D_s K$

When a final state f can come from both a pure B^0 and a pure $\overline{B}^0$, the amplitudes for the direct decay $B^0 \to f$ and the mixing induced sequence $B \to \overline{B}^0 \to f$ can interfere. A time dependent CP-violating effect can thus appear. Consider the following decay widths [1]:

$$\Gamma_1 = \Gamma(B \to f) = |M|^2 e^{-t} \left(\cos^2(xt/2) + \rho^2 \sin^2(xt/2) - \rho \sin(\phi+\delta)\sin(xt)\right)$$

$$\Gamma_2 = \Gamma(\overline{B} \to \overline{f}) = |M|^2 e^{-t} \left(\cos^2(xt/2) + \rho^2 \sin^2(xt/2) + \rho \sin(\phi-\delta)\sin(xt)\right)$$

$$\Gamma_3 = \Gamma(B \to \overline{f}) = |M|^2 e^{-t} \left(\rho^2 \cos^2(xt/2) + \sin^2(xt/2) - \rho \sin(\phi-\delta)\sin(xt)\right)$$

$$\Gamma_4 = \Gamma(\overline{B} \to f) = |M|^2 e^{-t} \left(\rho^2 \cos^2(xt/2) + \sin^2(xt/2) + \rho \sin(\phi+\delta)\sin(xt)\right),$$

where $M = \langle f|B\rangle$, $M' = \langle f|\overline{B}\rangle$, $\rho = |M'/M|$, $x = \Delta m/\Gamma$, δ is the strong phase difference between the two decays $B \to f$ and $B \to \overline{f}$, and ϕ is the relative CKM phase of the two decay amplitudes.

The time-dependent CP asymmetry is given by:

$$\begin{aligned} A_{CP}(t) &= \frac{[N(B\to f) + N(B\to \overline{f})] - [N(\overline{B}\to f) + N(\overline{B}\to \overline{f})]}{[N(B\to f) + N(B\to \overline{f})] + [N(\overline{B}\to f) + N(\overline{B}\to \overline{f})]} \\ &= \frac{\Gamma_1 + \Gamma_3 - \Gamma_2 - \Gamma_4}{\Gamma_1 + \Gamma_3 + \Gamma_2 + \Gamma_4} \\ &= \frac{2\rho}{\rho^2+1}\cos(\delta)\sin(\phi)\sin(xt)\ . \end{aligned}$$

The CP asymmetry is optimized if $2\rho/(\rho^2+1) \approx 1$, ie. the branching fractions of the decays into f and $\overline{f}$ are of the same order of magnitude.

A particularly useful case is where the B_s decays into the final states $f \equiv D_s^+ K^-$ and $\overline{f} \equiv D_s^- K^+$. Fig. 4 shows these two processes. These interfere with the mixing induced processes. The branching fractions are expected to both be $\sim 10^{-4}$ and in this case the weak angle $\phi = \gamma$. From a time-dependent study the quantities ρ, $\sin(\gamma+\delta)$ and $\sin(\gamma-\delta)$ can be extracted. The quantity $\sin\gamma$ can be extracted up to a 2-fold ambiguity. It is assumed that the value of x_s will have been determined in a separate measurement.

This method requires us to measure the time dependent asymmetry. Note that the final state is almost identical to the more prolific mode $D_s^+\pi^-$, which we have analyzed in the previous section for our B_s mixing study. Clearly, the particle identification is crucial here.

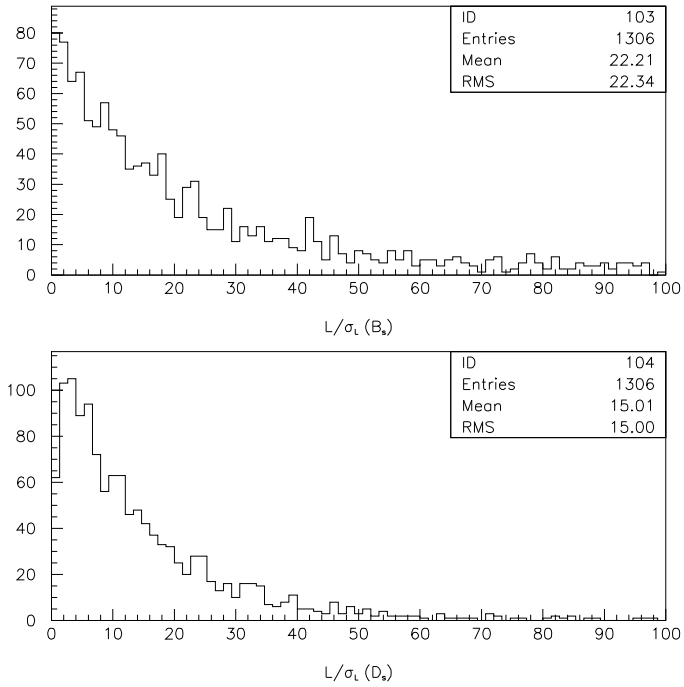

Figure 5: (a) $L/\sigma_L(B_s)$, (b)$L/\sigma_L(D_s)$

In this case $\rho = |A(B_s \to D_s^+ K^-)/A(B_s \to D_s^- K^+)|$, and the weak phase difference is γ. From a time-dependent measurement of the 4 decay rates $B_s \to D_s^+ K^-$, $B_s \to D_s^- K^+$, $\overline{B}_s \to D_s^- K^+$ and $\overline{B}_s \to D_s^+ K^-$ one can extract the quantities $\sin(\gamma + \delta)$, $\sin(\gamma - \delta)$ and ρ.

The main handle we have at triggering on and reconstructing these decays is the detachment of the secondary B_s and tertiary D_s decay verticies. The distributions of detachment length divided by the resolution in the detachment L/σ_L are shown in Fig 5. We require $L/\sigma_L(D_s) > 4.0$ and $L/\sigma_L(B_s) > 4.0$.

The combined geometric acceptance and reconstruction efficiency of these modes is 3.6% with a signal to background of 10:1. The trigger efficiency is 70% after all other cuts have been applied. (We used both the $\phi\pi$ and K^*K decay modes of the D_s.) Using branching ratios given by Aleksan et al. [1] and a tagging efficiency of 15% we expect a total of 800 tagged events (sum of 4 decay modes) in 10^7 s.

The CP asymmetry is diluted by time smearing, mistagging and background. The time resolution was found to be $\sigma_t = 0.047$ ps. We assume a mistag rate of 25% including mistagging due to the mixing of the other B.

The proper time resolution must be small to resolve the B_s oscillations. Fig. 6 is a plot of the generated proper time minus the reconstructed proper time for events passing the cuts described above. The proper time is calculated from the decay length where the decay point of the B_s comes from the vertex fit of the D_s with the K. A Gaussian fit to the $t_{gen} - t_{res}$ distribution gives $\sigma_t = 0.047$ psec for the $D_s \to \phi\pi$ mode and $\sigma_t = 0.055$ for the $D_s \to K^*K$ mode. Given that $\tau_{B_s} = 1.60$ psec, then $\sigma_t/t = 0.03$ (0.034 for the K^*K mode).

We estimated the accuracy in determining γ as follows. First, a set of "events" (*ie.* proper times) was generated, split into the 4 decay modes with correct time distributions. The values of the parameters were chosen to be $x_s = 20.0$, $\rho = 0.5$, $\gamma = 1.3(74.5\,\mathrm{deg})$ and $\delta = 0.4(22.9\,\mathrm{deg})$. Theoretically, the strong phase δ is expected to be small [2]. A fit was then done to confirm that we can get back the input values for ρ, $\sin(\gamma + \delta)$ and $\sin(\gamma - \delta)$.

Next a series of studies are done to see how finite time resolution, mistagging and background affect the fitted values of the parameters.

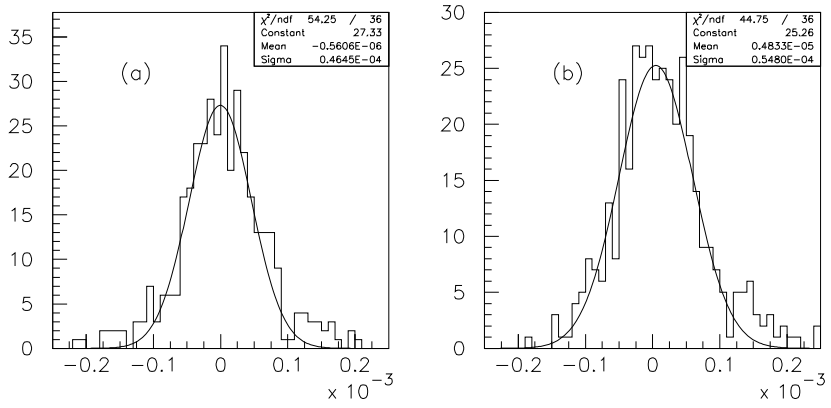

Figure 6: Proper Time Resolution for B_s : $t_{gen} - t_{rec}$ (nsec) (a)$\phi\pi$ mode (b) K^*K mode

- The proper times were generated, then smeared with a Gaussian of width $\sigma_t = 0.03\tau$. and a cut-off at low t simulated an L/σ_L cut: $t_{min} = 0.25\tau$
- The proper times were generated and a fraction were assigned to come from the "wrong flavor" parent. A mistag fraction of 25% is used. This includes mistagging due to mixing of the other B as well as other sources such as the decay chain $b \to c \to \mu$.
- Background events with a pure exponential time distribution are added to the "signal" events. The background is assumed to have the same lifetime as the signal.
- All the dilution factors are used.

In the absence of dilution factors the probability function is of the form:

$$P_1(t) = e^{-t}\{\cos^2(xt/2) + \rho^2 \sin^2(xt/2) - \rho \sin(\gamma + \delta)\sin(xt)\}$$

In the presence of dilution factors the following changes are made to the probability function:
(a) to correct for time smearing:

$$\begin{aligned} P_1^{'}(t) &= \int_{-\infty}^{\infty} dt^{'} \frac{e^{-(t-t^{'})^2/2\sigma^2}}{\sqrt{2\pi}\sigma^2} P_1(t) \\ &= e^{\sigma^2/2} e^{-t}[\cos^2(x(t-\sigma^2))(1 + e^{-x^2\sigma^2/2} + \rho^2(1 - e^{-x^2\sigma^2/2})) + \\ &\quad \sin^2(x(t-\sigma^2))(1 - e^{-x^2\sigma^2/2} + \rho^2(1 + e^{-x^2\sigma^2/2})) + \sin(x(t-\sigma^2))\sin(\gamma+\delta)], \end{aligned}$$

(b) to correct for background:

$$P_1^{''}(t) = P_1^{'}(t) + e^{-t}B, \tag{3}$$

(c) to correct for mistagging:

$$P_1^{'''}(t) = (1-w)P_1^{''}(t) + wP_4^{''}(t), \tag{4}$$

The value of $\sin\gamma$ can be extracted from $\sin(\gamma+\delta)$ and $\sin(\gamma-\delta)$ with a 4-fold ambiguity which reduces to a 2-fold ambiguity if it is assumed that $\sin\gamma > 0$. This still leads to a 4-fold ambiguity in the value of γ. If the true value of $\sin(\gamma+\delta)$ or $\sin(\gamma-\delta)$ is close to 1.0 then the fitted values may be outside the physically allowed region. In particular, this is likely when the number of events is small and hence the errors are large.

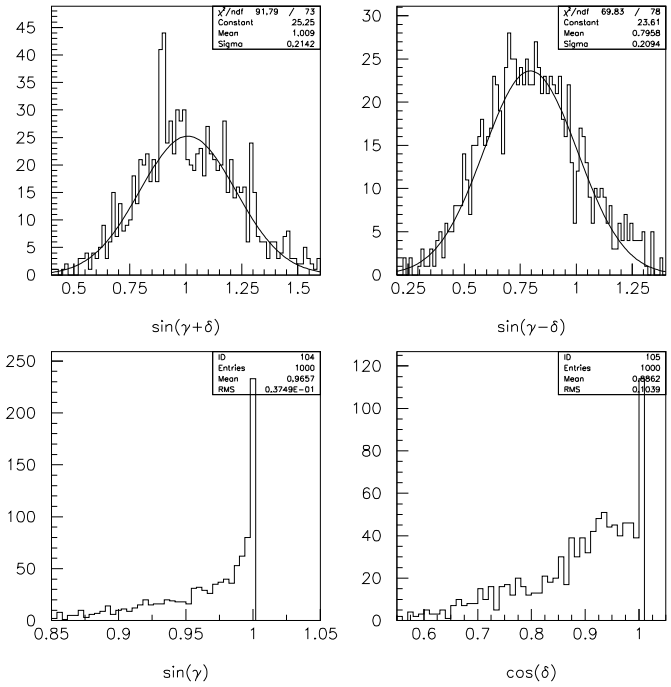

Figure 7: Fitted values of $\sin(\gamma+\delta)$, $\sin(\gamma-\delta)$, $\sin\gamma$ and $\cos\delta$. Input parameters $\sin(\gamma+\delta) = 0.992$, $\sin(\gamma-\delta) = 0.783$, $\sin\gamma = 0.964$, $\cos\delta = 0.921$

In order to study the obtainable accuracy on γ we ran 1000 "experiments," each with a signal of 1000 events where we fitted $\sin(\gamma+\delta)$ and $\sin(\gamma-\delta)$ and then calculated $\sin\gamma$ and $\cos\delta$, setting $\sin(\gamma+\delta)$ and $\sin(\gamma-\delta)$ to be equal to 1.0 if the fitted value was greater than 1.0. The results are shown in Figs. 7 and 8.

If $x_s = 20$ and $\rho = 0.7$ (from Aleksan's branching ratios) then it will be possible to measure $\sin(\gamma+\delta)$ and $\sin(\gamma-\delta)$ with a statistical error of $\approx \pm 0.2$ in one year of running at $\mathcal{L} = 5 \times 10^{31}\mathrm{cm}^{-2}\mathrm{s}^{-1}$. The largest potential experimental problem with this method occurs when x_s is near 60. Then the time smearing dominates the error and the measurement error increases substantially.

1.2.2 $B^- \to K^- D^0$

In the decay $B^- \to K^- D^0$ a large CP asymmetry can result from the interference of the decays $B^- \to K^- D^0, D^0 \to f$ and $B^- \to K^- \overline{D}^0, \overline{D}^0 \to f$, where f is a doubly Cabibbo suppressed decay of the D^0 (for example $f = K^+\pi^-, K\pi\pi$, etc.) [3]. Since $B^- \to K^- \overline{D}^0$ is color-suppressed and $B^- \to K^- D^0$ is color-allowed, the overall amplitudes for the two decays are expected to be approximately equal in magnitude. The weak phase difference between them is γ. To observe a CP asymmetry there must also be a non-zero strong phase between the two amplitudes.

We can define the following quantities:

$$a(K) = \mathcal{B}(B^- \to K^- D^0), \quad b(K) = \mathcal{B}(B^- \to K^- \overline{D}^0), \quad c(f_i) = \mathcal{B}(D^0 \to f_i),$$
$$c(\overline{f}_i) = \mathcal{B}(D^0 \to \overline{f}_i), \quad d(K, f_i) = \mathcal{B}(B^- \to K^-[f_i]), \quad \overline{d}(K, f_i) = \mathcal{B}(B^+ \to K^+[\overline{f}_i]),$$

where $i = 1, 2$ refers to two distinct final states of which at least one is not a CP eigenstate. The quantities $a(K) = \mathcal{B}(B^- \to K^- D^0)$, $c(f_i) = \mathcal{B}(D^0 \to f_i)$, $c(\overline{f}_i) = \mathcal{B}(D^0 \to \overline{f}_i)$, $d(K, f_i) = \mathcal{B}(B^- \to K^-[f_i])$ and $\overline{d}(K, f_i) = \mathcal{B}(B^+ \to K^+[\overline{f}_i])$ are assumed to be known. The branching ratio $b(K) = \mathcal{B}(B^- \to K^- \overline{D}^0)$, however, is not known.

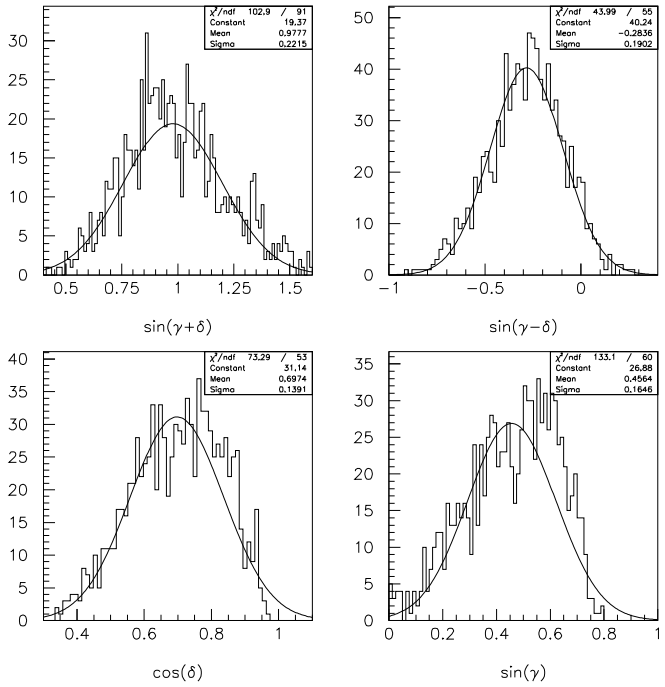

Figure 8: Fitted values of $\sin(\gamma+\delta)$, $\sin(\gamma-\delta)$, $\sin\gamma$ and $\cos\delta$. Input parameters $\sin(\gamma+\delta) = 0.969$, $\sin(\gamma-\delta) = -0.276$, $\sin\gamma = 0.497$, $\cos\delta = 0.697$

The total strong phase difference is $\xi^K_{f_i} = \zeta_K + \delta_{f_i}$, where

$$\zeta_K = \frac{1}{2}\arg\left[\mathcal{M}(B^- \to K^- D^0)\mathcal{M}(B^- \to K^-\overline{D}^0)^*\mathcal{M}(B^+ \to K^+ D^0)^*\mathcal{M}(B^+ \to K^+\overline{D}^0)\right] ,$$

and δ_{f_i} is the strong phase difference between $D^0 \to f_i$ and $\overline{D}^0 \to f_i$,

$$\delta_{f_i} = (\mathcal{M}(D^0 \to f_i)\mathcal{M}(\overline{D}^0 \to f_i)^*),$$

which can be large for non-CP eigenstates f_i.

The expressions for $d(K, f_i)$, $\overline{d}(K, f_i)$ written in terms of the strong phases and γ gives four equations

$$\begin{aligned} d(K, f_i) &= a(K)c(f_i) + b(K)c(\overline{f}_i) + 2\sqrt{a(K)b(K)c(f_i)c(\overline{f}_i)}\cos(\xi^K_{f_i} + \gamma) \\ \overline{d}(K, f_i) &= a(K)c(f_i) + b(K)c(\overline{f}_i) + 2\sqrt{a(K)b(K)c(f_i)c(\overline{f}_i)}\cos(\xi^K_{f_i} - \gamma) \end{aligned}$$

and four unknowns $\{\xi^K_{f_1}, \xi^K_{f_2}, b(K), \gamma\}$ that can be found up to discrete ambiguities. The measurement of additional decay modes can be used to help reduce the number of ambiguities.

It is necessary, therefore, to measure the branching ratio $\mathcal{B}(B^- \to K^- f_i)$ for at least 2 different states f in order to determine γ up to discrete ambiguities. We are assuming that the doubly Cabibbo suppressed decay rates $\mathcal{B}(D^0 \to f_i)$ will be well measured before BTeV, or we will have to measure them.

We have examined the decay modes $B^- \to K^-[K^+\pi^-]$ and $B^- \to K^-[K^+3\pi]$. The combined geometric acceptance and reconstruction efficiency was found to be 4% for the $K\pi$ mode and 3.4% for $K3\pi$ with a signal to background of about 1. The trigger efficiency is approximately 70% for both modes. The expected number of $B^\pm$ events in 10^7 s is 190 in the $K\pi$ mode and 320 in the $K3\pi$ mode. With this number of events we expect to be able to measure γ (up to discrete ambiguities) with a statistical error of about 20^o in one year of running at $\mathcal{L} = 5 \times 10^{31}\mathrm{cm}^{-2}\mathrm{s}^{-1}$. The overall sensitivity depends on the actual values of γ and the strong phases.

1.2.3 $B \to K\pi$

This method uses the branching ratios of the decays $B^+ \to \pi^+ K^0$ and $B^0 \to \pi^- K^+$ and their complex conjugates as explained in a recent paper by Gronau and Rosner [4].

The decay $B^+ \to \pi^+ K^0$ proceeds only through a penguin amplitude and the decay $B^0 \to \pi^- K^+$ proceeds through both penguin and tree amplitudes. Ignoring electroweak penguin contributions, the penguin amplitudes in the charged and neutral B decays to $K\pi$ are equal.

It is usful to define

$$R \equiv \frac{\Gamma(B^0 \to K^+\pi^-) + \Gamma(\overline{B}^0 \to K^-\pi^+)}{\Gamma(B^+ \to K^0\pi^+) + \Gamma(B^- \to \overline{K}^0\pi^-)}$$

$$A^{'} \equiv \frac{\Gamma(B^0 \to K^+\pi^-) - \Gamma(\overline{B}^0 \to K^-\pi^+)}{\Gamma(B^+ \to K^0\pi^+) + \Gamma(B^- \to \overline{K}^0\pi^-)}.$$

An expression for γ can be given in terms of R, $A^{'}$ and the ratio of tree to penguin amplitudes $r \equiv |T|/|P|$.

If we define δ to be the phase difference between the penguin and tree amplitudes, the ratios R and $A^{'}$ can be rewritten :

$$R = 1 - 2r\cos\gamma\cos\delta + R^2$$

$$A^{'} = 2r\sin\delta\sin\gamma$$

Combining these equations to eliminate δ we get

$$R = 1 + r^2 \pm \sqrt{4r^2\cos^2\gamma - A^{'2}\cot^2\gamma}$$

Fleischer and Mannel[5] have claimed that if $R < 1$ a useful bound can be obtained regardless of the value of r or δ:

$$\sin^2\gamma \leq R$$

If we have information on r we can get a more precise estimate of γ.

CLEO has determined $R = 0.65 \pm 0.40$, which suggests that the ratio could be less than 1.0 [6]. If this result holds with improved statistics then this method compliments other methods in that it will begin to exclude some of the region around $\gamma = \pi/2$.

Much attention was generated by the Gronau Rosner paper. Severe criticism was given by Gerard and Weyers [7] who contented that isospin was violated. Their criticism, however, was based on a quasi-elastic scattering assumption, which is not necessarily valid. Falk et al. [8] have shown that contributions to $B^+ \to \pi^+ K^0$ from rescattering of channels such as $B^+ \to \pi^0 K^+$ lead to a modification of the Fleischer-Mannel bound:

$$\sin^2\gamma \leq R(1 + 2\epsilon\sqrt{1-R})$$

where ϵ is the ratio of the rescattered amplitude to the penguin amplitude. They estimate $\epsilon = O(0.1)$. This rescattering contribution can be determined by measuring the K^+K^- final state branching ratio, which BTeV is well equipped to do. Other authors have made similar comments [9] [10].

The combined geometric acceptance and reconstruction efficiency of the $B^+ \to \pi^+ K^0$ mode is 4% and the trigger efficiency is 40%. The signal to background in the $K^\pm\pi^\mp$ mode is better than 1:1. However, the background study in the $K_s\pi^\pm$ modes has not yet been done. The reconstruction efficiency and trigger efficiency for the $B^0 \to \pi^- K^+$ mode are assumed to be the same as for $B^0 \to \pi^+\pi^-$[11].

We expect to reconstruct 3600 $B^\pm$ and 36000 $B^0/\overline{B}^0$ in 10^7 s of running at $\mathcal{L} = 5 \times 10^{31}\mathrm{cm}^{-2}\mathrm{s}^{-1}$. Gronau and Rosner [4] have estimated that a 5° precision in γ can be achieved with 2400 events in each channel. This of course, doesn't take into account the above mentioned theoretical criticisms of the technique. BTeV more than satisfies this level of events. Estimates of the uncertainties which can be achieved on $\sin\gamma$ are in preparation.

Table 2: BTeV event sample after one year of running at luminosity of $5 \times 10^{31}\mathrm{cm}^{-2}\mathrm{s}^{-1}$. Simulations were done using the BTeV baseline detector that was described in the EoI.

Channel	Observed mode	Untagged events/year	Physics
$B_d^0 \to J/\psi K_s^0$	$\mu^+\mu^-\pi^+\pi^-$	28000	$\sin 2\beta$
$B_d^0 \to \pi^+\pi^-$	$\pi^+\pi^-$	17000	$\sin 2\alpha$
$B_s^0 \to D_s K$	$\phi\pi K; \phi \to K^+K^-$	2350	$\sin\gamma$
$B_s^0 \to D_s K$	$K^{0*}KK$	3000	$\sin\gamma$
$B_d^0 \to K^- D^0$	$K^-[K^+\pi^-]$	190	γ
$B_d^0 \to K^- D^0$	$K^-[K^+3\pi]$	320	γ
$B_d^0 \to \pi^- K^+$	$\pi^- K^+$	36000	γ
$B^+ \to \pi^+ K^0$	$\pi^+ K_s^0$	3600	γ
$B_s^0 \to D_s\pi$	$\phi\pi^-\pi^+; \phi \to K^+K^-$	17000	x_s
$B_s^0 \to J/\psi \bar{K}^{0*}$	$\mu^+\mu^- K^-\pi^+$	1470	x_s
$B^\pm \to K^\pm\mu^+\mu^-$	$K^\pm\mu^+\mu^-$	300	SM rare decay

1.2.4 Summary of techniques to measure γ

Our simulations show that BTeV is in the extraordinary position of being able to acquire meaningful event samples using three different techniques to measure γ. The event samples we predict in one year of running at low luminosity are given in Table 2, along with several other modes for comparison.

It is important to measure γ using more than one technique, since all of the above methods have some discreet ambiguities associated with them.

References

[1] "Determining the CP-violating phase γ",R. Aleksan, I. Dunietz, B. Kayser, Z. Phys C **54**, 653-659 (1992); R. Aleksan, B. Kayser and D. London, "In Pursuit of γ," DAPNIA/SPP 93-23, hep-ph/9312338.

[2] "Determination of the CP-violating phase γ by a sum over common decay modes to B_s and $\overline{B}_s$ ",R. Aleksan, A. Le Yaouanc, L. Oliver, O. Pene, J.-C. Raynal, Z. Phys C **67**, 251-260 (1995).

[3] D. Atwood, I. Dunietz and A. Soni, PRL 78, 3257(1997).

[4] M. Gronau and J. Rosner, CALT-68-2142, hep-ph/9711246 (November 1997).

[5] R. Fleischer and T. Mannel, hep-ph/9704423.

[6] CLEO Collaboration, Cornell report CLEO CONF 97-22, submitted to Lepton-Photon Symposium, Hamburg, Jully 1997; B. Behrens and J. Alexander at the *The Second International Conference on B Physics and CP Violation*, Honolulu, Hawaii, March 1997; F. Wurthwein at *Les Rencontres du Moriond:QCD and High Energy Hadronic Interactions*, Les Arcs, France, March 1997, hep-ex/9706010.

[7] J.-M. Gerard and J. Weyers, "Isospin amplitudes and CP violation in ($B \to K\pi$) decays," hep-ph/9711469 (1997).

[8] A. Falk, A. Kagan, Y. Nir and A. Petrov, JHU-TIPAC-97018 (December 1997).

[9] M. Neubert, "Rescattering Effects, Isospin Relations and Electroweak Penguins in $B \to \pi K$ Decays," hep-ph/9712224 (1997).

[10] D. Atwood and A. Soni, "The Possibility of Large Direct CP Violation in $B \to K\pi$-Like Modes Due to Long Distance Rescattering Effects and Implications for the Angle γ," hep-ph/9712287 (1997).

[11] BTev EOI (May 1997).

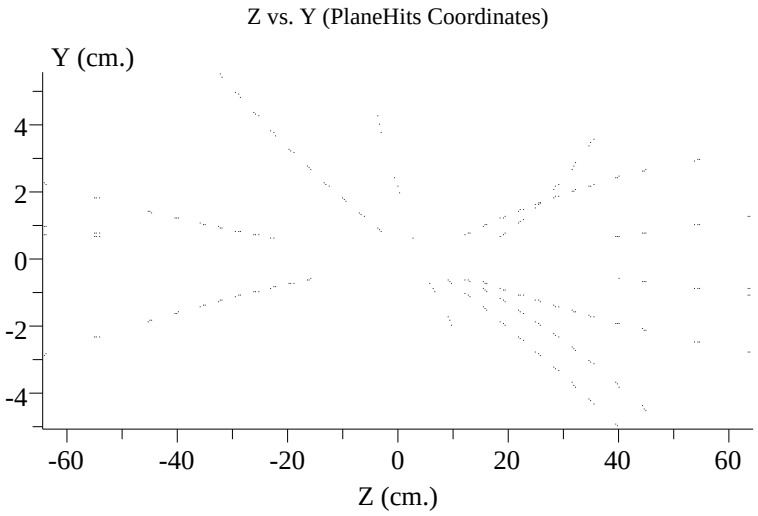

Figure 9: Pixel hits in Z-Y projection with no random noise from an MCFAST simulation

1.3 Trigger Studies

The goal of the trigger is to reconstruct tracks and find vertices in every interaction, up to a luminosity of $2 \times 10^{32}\text{cm}^{-2}\text{sec}^{-1}$. It must be capable of reducing the trigger rate by a factor between a hundred and a thousand. We employ parallelism both at the subevent level and at the event level. The detector layout has "stations" consisting of three planes of pixel detectors. Processors organize the hits in each triplet of planes into "station hits". Still at the subevent level, individual processors work on the station hits from a "ϕ" slice of the detector to form tracks. At the event level, tracks from individual slices are brought together in a vertex finder node. The corresponding algorithms for these various stages are described in detail elsewhere [1],[2]. In this note, we are reporting on:

- Performance studies of this baseline algorithm, in presence of backgrounds; and
- Performance studies on the baseline trigger in the presence of multiple interaction per crossings.

We remind the reader that these studies are performed using a full hit-level simulation and a full pattern recognition algorithm. Although the final criteria for triggering will depend on the luminosity, the algorithm that we have implemented runs well on crossings which have as many as 3 interactions in them.

1.3.1 Uncorrelated Noise Study

Here we investigate the effects on the trigger algorithm of adding random noise to the pixel detector. This study was performed by throwing random hits from a Poisson distribution of average value <N>, uniformly distributed over the area of each plane. Electronic noise or neutrons could cause this kind of distribution.

Fig. 9 shows an event with no random noise. Fig. 10 shows the same event, but with an average of 25 noise hits distributed randomly over each of the 93 pixel planes.

Fig. 11 shows the efficiency for minimum bias events, which we want the trigger to reject, and signal events (in this case events with a decay $B^o \to \pi^+\pi^-$), which we want the trigger to accept, plotted against the average number of random noise hits per plane.

We believe that it should be possible, and the experience with existing detectors bears this out, to achieve random noise levels below 10^{-5} if hot channel suppression is included in the pixel readout system. The result of our study is that the efficiency and rejection of the baseline trigger were preserved up to $\approx$<N>=100, which corresponds to a contribution of random background to the occupancy of 10^{-4}. We expect the detector to have a much lower noise level than this. However, it was observed that processing time did get somewhat longer when the number of hits rose above a mean of 25. We plan to revisit this issue soon.

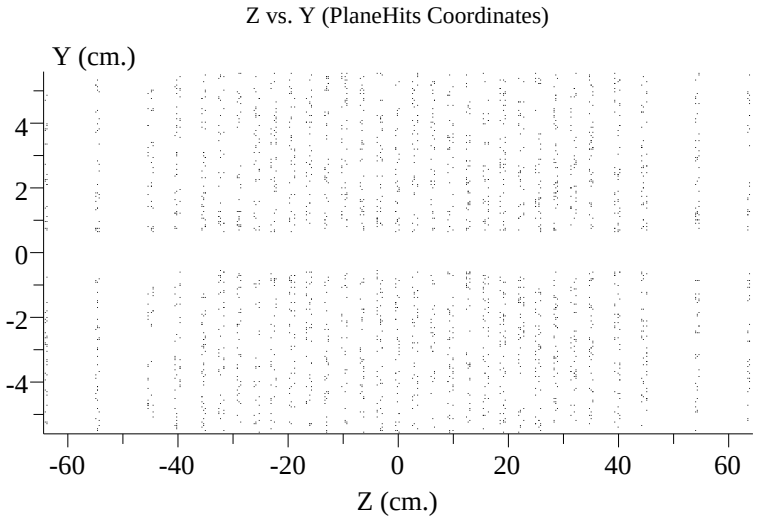

Figure 10: Pixel hits in Z-Y projection with an average of 25 random noise hits from an MCFAST simulation

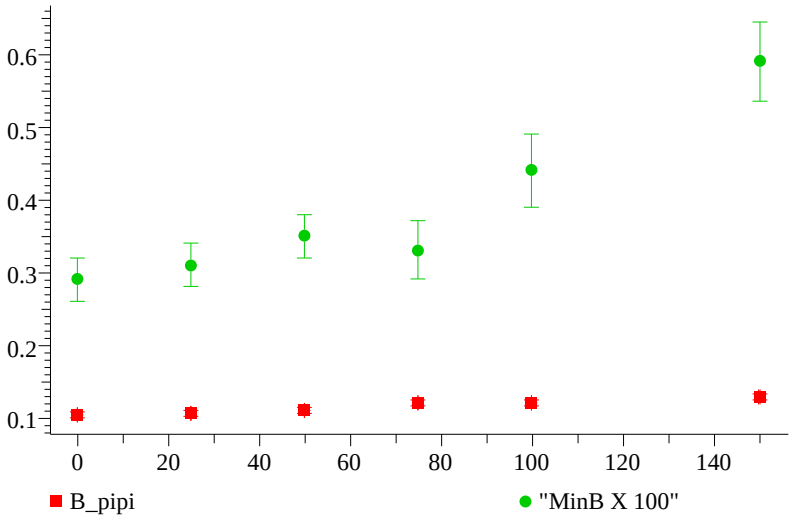

Figure 11: Efficiency vs average number of random noise hits for minimum bias and B events.

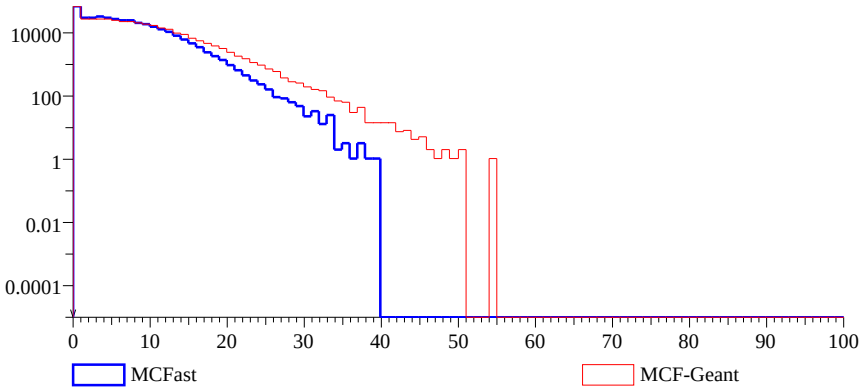

Figure 12: Hit multiplicity for minimum bias events in GEANT simulation and MCFAST simulation

1.3.2 Correlated Noise Study

In this study, we used GEANT to simulate the events and turned on all its physics processes. This led to additional hits from hadronic interactions, photon conversions, decays in flight, and curlers (a.k.a loopers). Fig. 12 shows that average number of hits per plane rises by about 20% from 5.6 hits/plane to 6.8 hits/plane. A degradation of 1.5 is observed in the overall rejection capability of the trigger.

There are other sources of correlated noise. For example, beam-gas interactions or beam halo particles might leave long tracks in the detector. Although the time between crossings is long, there may still be background hits from previous crossings whose source and distribution we are not currently modeling. None of these is expected to be a serious problem but more work does need to be done to prove this definitively.

1.3.3 Multiple Interactions per Crossing Study

In order to achieve the desired statistical precision, BTeV will begin to run at a luminosity of 5×10^{31} but we will eventually want to run at a luminosity of at least 2×10^{32}. The lower luminosity creates an average of 0.5 inelastic interactions per crossing, while the higher luminosity generates an average of two. Because the Tevatron will have only 108 bunches, this means that the experiment, and in particular the trigger, must be able to handle multiple interactions per crossing.

At the time of the Fermilab PAC meeting in June of 1997, we had just barely started to study this problem. Since then, we have made significant progress, which we describe below. The bottom line is that, even in the presence of multiple interactions, the trigger continues to give good efficiency for states with B-decays while providing good rejection against minimum bias events because the occupancy of the pixel vertex detector is very low, and the luminous region of the Tevatron is long.

In order to achieve good results when there are multiple primary vertices, we had to make only a small refinement to the trigger algorithm: we put an **upper limit** on the impact parameter (with respect to the primary vertex) which is used to define secondary vertex track candidates. This prevented non-verticizing tracks associated with one primary interaction from automatically appearing as 'detached' when compared to another primary vertex.

Here we present only a brief summary of the results of an extensive study [3].

Performance on Single Interaction Crossings

The average number of tracks per interaction (primary and secondary) which pass through at least three stations of the pixel detector is 19.8 for minimum bias events and 28.8 for $B^o \to \pi^+\pi^-$ events (which will be called B events from now on). After a set of cleanup cuts on the tracks, the average multiplicity of tracks that the trigger uses in the vertex search is 10.1 for minimum bias events and 14.2 for B events. For tracks passing through at least 3 stations, the efficiency for track finding reaches an asymptote of about 85% by a momentum of 10 GeV/c. Two additional cuts are placed on tracks which are candidates for use in the primary vertex: they must have a transverse momentum of less than 1.2 GeV/c; and they must

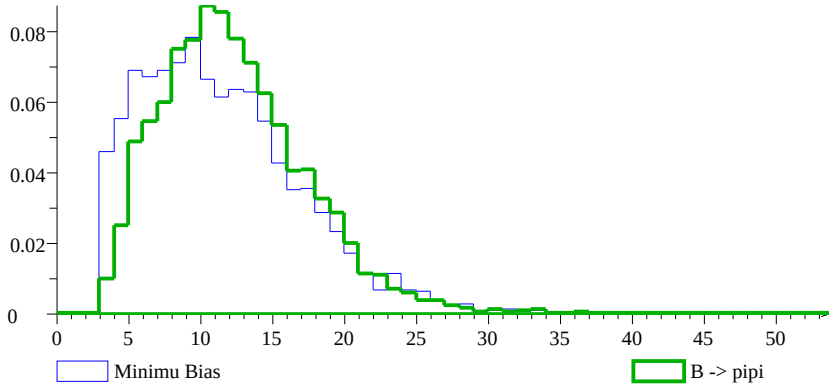

Figure 13: The track multiplicity distribution in the primary vertex, for single interaction crossing. The average is 11.4 for minimum bias events, and 12.03 for $B \to \pi\pi$.

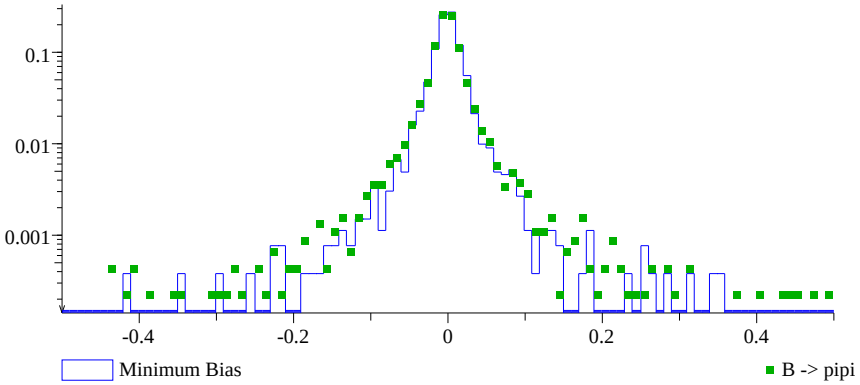

Figure 14: The Z primary vertex resolution, for a single primary vertex event. The width of these distribution are 370 μm and 444 μm for minimum bias and $B \to \pi\pi$ samples respectively.

satisfy the requirement that they intersect the nominal beam line within the luminous region. With these requirements, the multiplicity of primary vertex tracks found by the trigger algorithm in a crossing with exactly one interaction is given in Fig. 13 for minimum bias and B events. The Z resolution of the primary vertex is given in Fig. 14.

At least 3 tracks are required to form a primary vertex. As a consequence of this cut and the transverse momentum cut, the probability to find a second, false, primary vertex is very small, only 0.05%, in minimum bias events. The 'leftover' track multiplicity after primary vertex formation is very different for minimum bias and B events. If one applies an additional detachment cut on the normalized impact parameter, $\frac{\sigma_b}{b}$, of 3 and a transverse momentum cut, $P_t > 0.5$ GeV/c, one has reconstituted the analysis we presented in June 1997. To deal with multiple interactions, we added the requirement that the 'detached track candidate' not be **too far from the primary vertex** – the impact parameter b must be less than 0.2 cm from the primary. Then, one obtains the distribution in Fig. 15.

Table 3 shows the trigger acceptance for minimum bias events and B events for single interaction crossings. Our goal for Level I was to accept fewer than ≈1% of minimum bias events, which is achieved by all conditions, except for those in the top line.

Performance on Multiple Interaction Crossings

Fig. 16 shows the number of vertices reconstructed by the trigger algorithm for 2.0, 2.5, and 3.5 average number of interactions per crossing. These plots show that the number of reconstructed vertices is well correlated to the number of generated vertices even in these busy events. The distribution can be understood

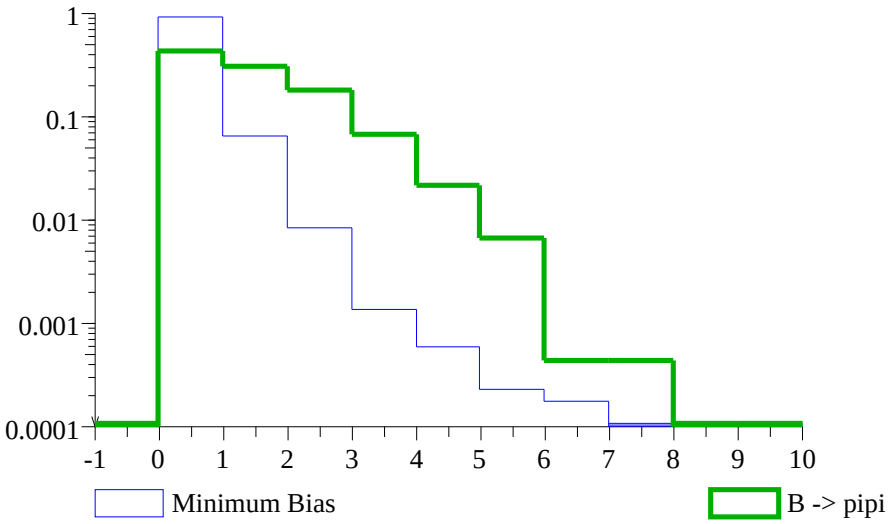

Figure 15: The detached, high P_t, track multiplicity for both samples. The average track multiplicity for minimum bias (B) is 0.6 (1.5).

Table 3: The Trigger Acceptance (%) for single interaction crossings, for the minimum bias sample and the $B \to \pi\pi$ sample, versus selection criteria (number of tracks detached from the primary, detachment cut, P_t on each detached track, and impact parameter upper limit in cm). The errors are statistical only.

Criteria	Minimum Bias	$B \to \pi\pi$
2 detached tracks ($3\sigma; P_t > 0.5$ GeV/c)	1.9 ± 0.1	28.9 ± 0.9
3 detached tracks ($3\sigma; ; P_t > 0.5$ GeV/c)	0.50 ± 0.04	11.0 ± 0.5
2 detached tracks ($3\sigma; P_t > 0.5$ GeV/c; $b_t < 0.2$)	1.02 ± 0.05	25.3 ± 0.9
3 detached tracks ($3\sigma; P_t > 0.5$ GeV/c; $b_t < 0.2$)	0.23 ± 0.02	9.5 ± 0.5

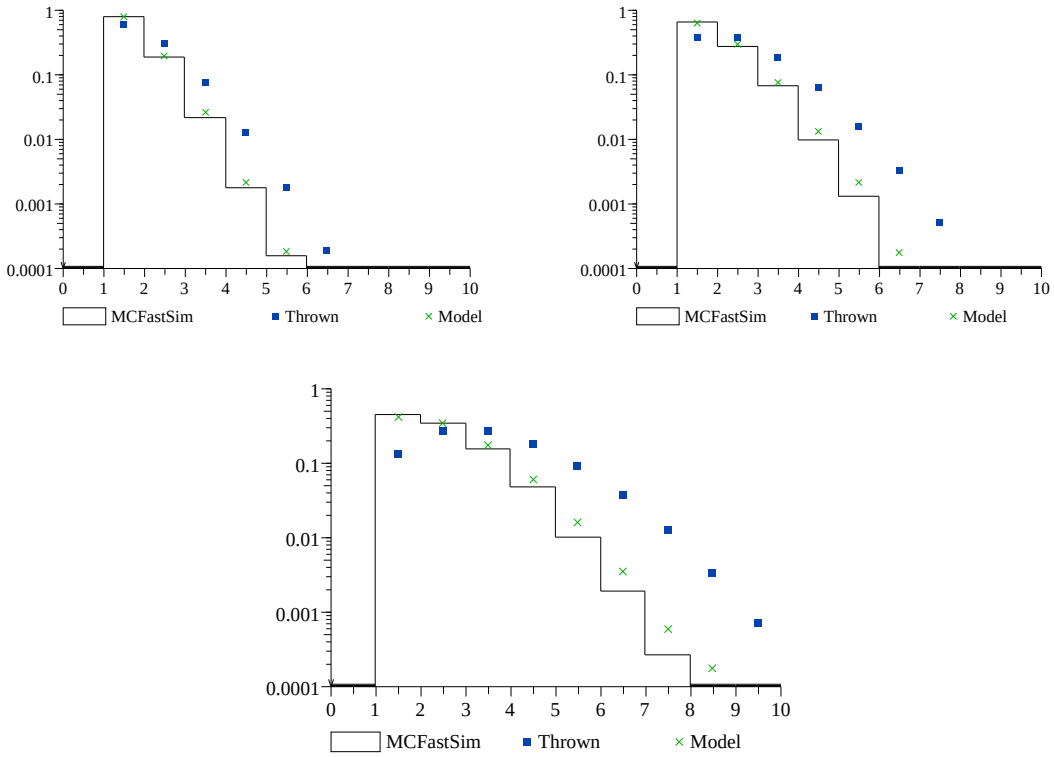

Figure 16: The primary vertex multiplicity distribution for three different average number of interaction per crossings. In all cases, at least one vertex is thrown and reconstructed. Top corresponds to $< 0.5 >$ additional inter./crossing (Poisson distributed); top-left, $< 1.0 >$ additional inter./crossing (top-right) and and $< 2.0 >$ additional inter/crossings (bottom). Also shown are the corresponding Poisson distributions for these averages (green filled squares) and the expected distribution assuming a fixed primary vertex reconstruction efficiency of 55 %.

as a Poisson distributed number of interactions with a fixed vertex finding efficiency of about 55%. The efficiency is low because the trigger is deliberately made insensitive to very soft collisions such as quasi-elastic and low multiplicity interactions (a good feature!) which are unlikely to contain B's.

Fig. 17 shows the degradation of the Z resolution as additional vertices are reconstructed in the crossing. By virtue of our algorithm, the most populated primary vertex is reconstructed first. As the track to vertex assignments proceeds, one finds the vertices which are less populated. However, the Z resolution remains acceptable even for the vertices found later and with lower multiplicity.

Fig. 18 shows the 'multiplicity distribution' of detached tracks for different number of reconstructed vertices when the average number of interactions per crossing is ≈ 2. The main point is that there is not a large tail of events in which the number of detached tracks begins suddenly to become troublesome as the number of reconstructed vertices increases. We observe that the efficiency for detecting B events does not degrade as the number of actual or reconstructed vertices increases. Fig. 19 shows the same distribution when the average number of interactions per crossing is 3.5 (much higher than we propose at present to run). We now see that the trigger rate begins to be dominated by crossings with three or more reconstructed vertices

The behavior of the total yield of B events per unit time and the probability of triggering on a crossing with at least one inelastic interaction is shown vs luminosity (in units of $10^{32}\,\mathrm{cm}^{-2}\,\mathrm{s}^{-1}$) in Fig. 20. (Here, we have used a trigger requirement of at least 3 tracks each missing the primary by $\geq 3\sigma$.) Ideally, one would expect the yield per unit time to increase linearly and it does increase roughly linearly as long as one does not restrict the number of interactions too severely. The probability for triggering on crossings with inelastic interactions does increase but stays below 1% up to a luminosity of 3×10^{32} if we allow at most three

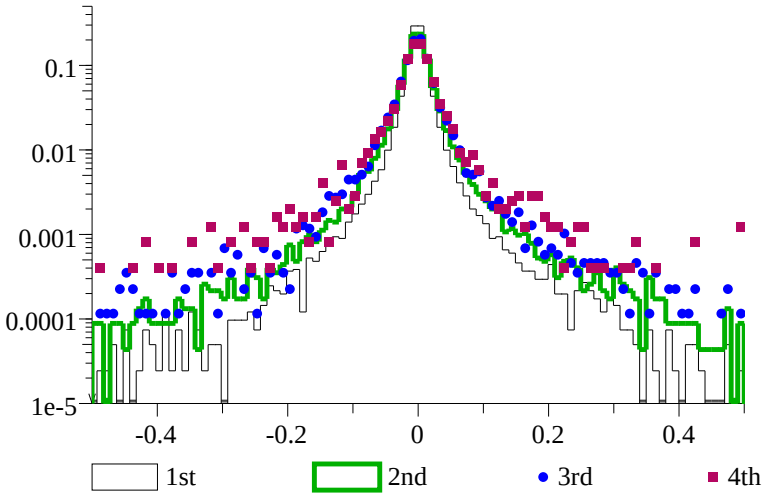

Figure 17: The Z position primary vertex resolution plot, running with an average of $\approx$ 3 interactions per crossing, for the first 4 vertices found in the event. All plots have been renormalized for comparison purposes. The width of these distributions are 322 μm, 460 μm, 545 μm and 632 μm for the first, second, third and fourth vertex found in the crossing. Note that the first histogram may corresponds to crossing with more than vertex.

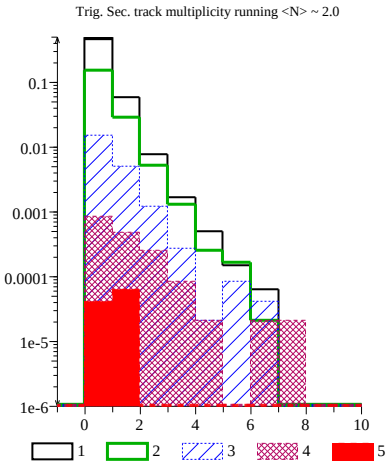

Figure 18: The detached track multiplicity distributions for different reconstructed primary vertex multiplicities, running at $\approx$ 2 interactions per crossing. The lower axis is the total number of detached tracks (3 σ detachment). The different hatchings represent the different number of reconstructed primary vertices. The vertical axis is the probability to find a given detached track multiplicity in the crossing.

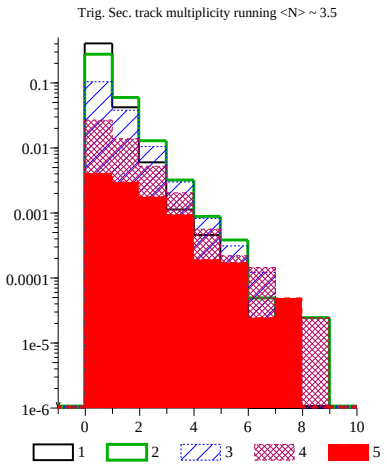

Figure 19: The detached track multiplicity distributions for different reconstructed primary vertex multiplicities, running at ≈ 3.5 interactions per crossing. The lower axis is the total number of detached tracks ($3\ \sigma$ detachment). The different hatchings represent the different number of reconstructed primary vertices. The vertical axis is the probability to find a given detached track multiplicity in the crossing.

reconstructed vertices. There are many additional requirements (such as the presence of a true secondary vertex rather than tracks missing the primary) that can be imposed at Level I to reduce the trigger rate even more.

Our first results on the performance of the baseline trigger in the presence of multiple interactions per crossing are quite encouraging. In essence,

- At moderate luminosity ($\approx 0.5 \times 10^{32}$) the trigger rate is not dominated by unresolved multiple vertices. In fact, if one wanted to run accepting only single vertex crossings (due for instance to limitation of the Level 2 input bandwidth), one would run at a higher luminosity where the probability to reconstruct more than one vertex is not negligible.

- If the Level 2 bandwidth is high enough, so that a Level 1 rejection factor of about one in a hundred is acceptable, one gains sensitivity by running above an average of 1 interaction per crossing provided we accept crossings with up to three interaction vertices.

Thus, we believe that it is possible to achieve a rejection against minimum bias events of 1/200 to 1/300 at Level 1 up to a luminosity of 10^{32} with good efficiency for B events. One can work above 10^{32} provided one can handle the data rate of falsely accepted minimum bias events into the Level II trigger or one can reduce the rate into Level II by adding more requirements on Level I. However, there is more work to be done in making the simulation more realistic and in refining the algorithm. Also, we need to estimate the required CPU power at a given stage of the reconstruction, to balance the data flow in the pipeline. We look forward to reporting further on this in the future.

References

[1] BTeV EOI (May 1997).

[2] These results are based on the work of R. Isik, W. Selove, and K. Sterner,"Monte Carlo Results for a Secondary-vertex Trigger with On-line Tracking," Univ. of Penn. preprint UPR-234E (1996).

[3] P. Lebrun, "On the Vertex Pattern Recognition in the BTeV Trigger," BTeV internal note 97/17 (1997).

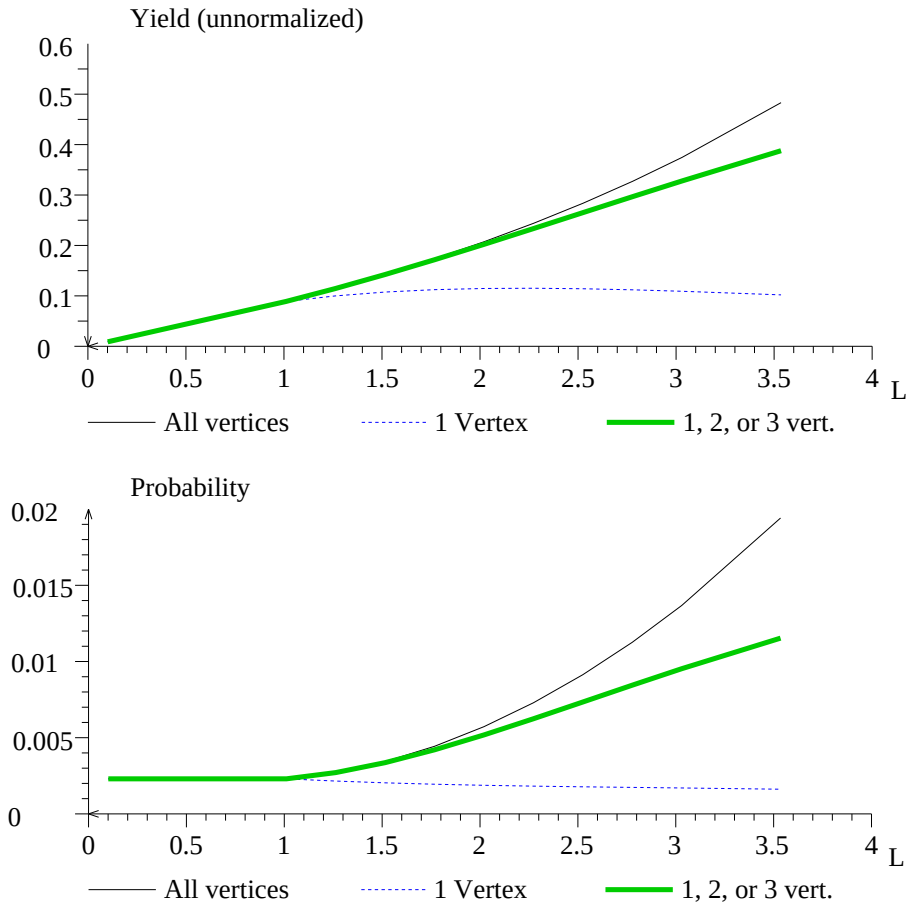

Figure 20: Top curve: The yield for events with $B^o \to \pi^+\pi^-$. Since the curves are not absolutely normalized, their important features are their shapes. Bottom curve: The absolute probability for triggering on crossings with inelastic interactions. For both plots, the lower axis is the luminosity in units of $10^{32}\,\mathrm{cm}^{-2}\,\mathrm{s}^{-1}$. The solid line is for events with greater then 1 reconstructed vertex; the dotted line, for events with one and only one reconstructed vertex; and the thick gray line for events 1, 2, or 3 reconstructed vertices.

1.4 Improvements to BTeV Simulation

One of the recommendations of the June Aspen meeting was that the BTeV collaboration improve its tracking and analysis programs. In this section, we describe progress in this area since June.

1.4.1 Improvements to MCFAST

Physics simulations for BTeV have been done using Pythia [1] and the detector simulation package MCFast [2]. Inside the MCFast simulation package, particle trajectories are traced through the detector and the outputs are smeared track parameters as well as hits. At the time of the submission of the BTeV EOI, the errors on the track parameters were always Gaussian and reflected contributions from multiple scattering and measurement error. Also included in the EOI simulation package were decays in flight, photon conversions, dE/dx, parameterized showers and simple hit generation in tracking devices and in the calorimetry. The package could also handle events with multiple interactions.

Several important features have been added to the detector simulation code since that time that make the simulation more realistic. We have added secondary interactions and have made an updated version of a geometry interface package that will read MCFast geometry files into the GEANT simulation package [3]. We have made further improvements to MCFast by adding improved tracing (in C^{++}), and a new fitter that is based on a Kalman filter that will allow us to examine errors from pattern recognition and other non-Gaussian effects.

1.4.2 Kalman Filter

In section 4.11 of the BTeV EOI a work plan for the BTeV simulation program was presented. Two of the projects in this work plan were improvements to the tracking simulation, namely the completion of the Kalman filter code and the simulation of errors in pattern recognition.

A Kalman filter [4], also known as a Billoir fitter [5], is a technique for the unbiased, optimal treatment of multiple scattering in a track fit. In an experiment, such as BTeV, in which vertexing is the critical off-line analysis tool, it is of the utmost importance to have such a fitter. In the above, the adjective "optimal" means that a Kalman filter produces an estimator of the track parameters which has the minimum variance of any linear estimator. To be precise, the properties of "unbiased" and "optimal" are only rigorously true when both the multiple scattering and the measurement errors are Gaussian. However for practical applications to HEP track fitting this is often a sufficiently good approximation.

Another important feature of the Kalman filter is that it executes in a time proportional to the number of hits on the track, whereas other unbiased, optimal methods of dealing with multiple scattering involve the inversion of large ($N_{\rm hit} \times N_{\rm hit}$) matrices, and execute in correspondingly longer times. While the Kalman filter can be used as the propagation step in a pattern recognition program, it is used here only as a final fitter; that is, another piece of MCFast assembles a list of hits and scattering surfaces which belong to one track and then passes that list to the Kalman filter.

At the time of the BTeV EOI the Kalman filter was not yet complete and physics analysis results presented therein were obtained using the following technique, based on ideas from TRACKERR [6]. (The trigger simulations have all been done using full pattern recognition and an independent track finding algorithm.) For each track, a list of hits and scattering surfaces was prepared. The Kalman filter inside MCFast was then used to compute the covariance matrix of the track parameters at the production vertex of the track. The track parameters were modeled by choosing a random 5-vector from the 5-dimensional Gaussian distribution described by the covariance matrix; this random 5-vector was then added to the generated track parameters. It should be emphasized that, in the limit of perfect pattern recognition, Gaussian multiple scattering and Gaussian measurement errors, this method is equivalent to the present method of using a Kalman filter to obtain the track parameters.

The weakness of the TRACKERR-like method, however, is that one cannot use it to investigate the effect of imperfect pattern recognition or the effects of non-Gaussian tails either in multiple scattering or in the hit resolution functions. With the completion of the Kalman filter these effects can now be investigated and a program to exploit this new code will soon be underway. For example, it is now possible to smear the hits with one resolution function and to use another resolution function in the fit. An important application of this is in the simulation of the pixel detectors, in which δrays can cause the cluster finding algorithm to return a biased center-of-charge.

The algorithm to simulate errors in pattern recognition has been designed and will be coded in the next few weeks. The goal is to simulate the class of tracks for which the pattern recognition is substantially correct but which also contain a small number of incorrect hits.

Of particular interest are those cases in which a pixel hit, close to the production point, has been incorrectly assigned to the track. Such tracks might arise from two tracks which are close to each other, from generic event confusion, from beam related backgrounds or even from delta rays. It is anticipated that such tracks will be a major source of false secondary vertex candidates and it is important to understand the magnitude of the false secondary backgrounds. In brief, the algorithm is to fully simulate the event, including all noise sources, and then to scan in the neighborhood of each hit on each track to build a list of nearby hits which might be confused for the correct one. Some fraction of the time one of the incorrect hits will be added to the list of hits to be passed to the fitter.

1.4.3 GEANT-based Simulation Package

The simulation group has developed an interface between GEANT and the **development** version of MCFast that will enable a more detailed simulation that meets the needs of the collaboration. Like MCFast, the Geant-based package is flexible and can be used for simulation and comparison of different detector geometries. Changing the detector geometry does not involve modification of the code and can be done by switching from one geometry database file to another. The package allows to take advantage of the full simulation of physics processes that is a feature of GEANT. The package uses exactly the same command, geometry, and event files as MCFast and allows straightforward comparison of results of parametrized and full simulation.

Most of the effort has been in the conversion of MCFast detector geometry representation into GEANT format. The package handles the same basic components that MCFast does, i.e. beampipe, magnets (dipoles and solenoids), including coils and yokes, Silicon vertex detectors, forward and central tracking chambers, calorimeters, absorbers, and muon chambers. The collaboration plans to continue to work on the package. The first task will be to improve the hit generation in the calorimeter and the tracking detectors.

We have used the package to do studies of the pixel detectors. These studies will be refined by the addition of more realistic hit generation in the vertex detector.

1.4.4 Studies of New Pixel Detector Designs

The process which makes the toughest demands on the pixel detector is the measurement of x_s, the mixing parameter in the B_s system. Current theoretical expectations are that the value should lie in the $20 \leq x_s \leq 60$ [7]. If x_s has a value in the neighborhood of 60, then the time corresponding to one quarter of an oscillation period is approximately 40 fs. This means that, if BTeV is to be sensitive to x_s over the full expected range, then the pixel detector must achieve a resolution on proper decay time in the neighborhood of $40fs$. The detector described in EOI obtained a mean time resolution of 45 fs for the decay mode $B_s \rightarrow \psi \overline{K}^{*0}$ and it is important to understand how this can be improved.

A systematic program was undertaken to understand how the time resolution and acceptance are affected by the following factors: the amount of multiple scattering in the pixel system; the spatial resolution in the short dimension of the pixel; the size of the vertical gap; and the overall layout of the detector. Two conclusions can be drawn from these studies.

1. The x_s reach is sensitive to small changes in the amount of multiple scattering in the pixel system, the spatial resolution of the pixels, and the size of the vertical gap between halves of the pixel planes. This implies that any modification to the design which degrades one of these properties must be accompanied by other changes to improve the performance.

2. The x_s reach is dramatically improved if the vertical gap between the upper and lower halves of the pixel planes is reduced or, even better, eliminated in favor of a small central hole for the beam to pass through. (This has always been understood but the improvement was more dramatic than expected.)

Finally, these statements are accompanied by the caveat that the background rejection of the trigger has not yet been checked with the square-hole design.

The specific pixel detector simulated for this study had a square hole, 1.2 cm on a side, at the center of the detector and the remainder of the horizontal gap was reduced to zero. The resolution remained uniform as $30/\sqrt{12}\mu$m throughout the active surface of the pixel planes. The y extent of the pixel planes was reduced so that the active area of this new detector was the same as that of the EOI detector.

When the decay mode $B_s \to \psi \overline{K}^{*0}$ was studied with this detector and the acceptance for signal events was found to improve by 70%. Moreover the mean time resolution dropped from about 45 fs to about 33 fs. These two effects dramatically improve the x_s reach of this mode, as is detailed in Section 1.1 and Fig. 3.

The remaining stages of this study are to map out the allowed region in the space of material thickness, pixel resolution, and the size and shape of the central hole. In addition, inserts of diamond pixel detectors will be investigated. These inserts would partially fill the central hole using a device which is more radiation-hard than silicon pixels.

References

[1] H. U. Bengtsson and T. Sjostrand, Comput. Phys. Commun. **46**, 43 (1987).

[2] P. Avery *et al*, "MCFast: A Fast Simulation Package for Detector Design Studies" in the Proceedings of the International Conference on Computing in High Energy Physics, Berlin, (1997) and http://fnpspa.fnal.gov/mcfast/mcfast_docs.html

[3] R. Brun *et al*"GEANT Detector Description and Simulation Tool", CERN Program Library Long Write-up, W5013.

[4] For example, see. M. Regler and R. Fruhwirth, "Reconstruction of Charged Tracks", in *Techniques and Concepts of High-Energy Physics V*, Plenum Publishing Corp., (1990), pp 407-501.

[5] P. Billoir, Nucl. Instr. and Meth. Phys. Res., Sect. A **225**, 352 (1984).

[6] http://heplibw3.slac.stanford.edu/FIND/FREEHEP/NAME/TRACKERR/FULL

[7] S. Stone, "THE Goals and Techniques of BTeV and LHC-B," to appear in proceedings of "Heavy Flavor Physics: A Probe of Nature's Grand Design", Varenna, Italy, July 1997; hep-ph/9709500.

[8] K.T. McDonald, "Maximum Likelihood Analysis of CP Violating Asymmetries", PRINCETON-HEP-92-04, Sep 1992. 12pp. Unpublished.

2 R&D Plan for FY98 (and beyond)

2.1 Simulation R&D Plans

2.1.1 Simulation Development and Detector Studies

The MCFast software developed for BTeV simulations has been a useful tool for studying the physics potential of the baseline detector. Several improvements to the current package are planned. During the coming year the BTeV simulation group plans to extend MCFast and the BTeV GEANT simulation to include more realistic hit generation. These updates will be used for simulating and studying the resolution and response of the pixel detector, the tracking chambers and the RICH detector. We plan to use these new tools to finalize our detector design.

We have already developed tools for studying pattern recognition in the tracking devices. We plan to use these new tools to make further studies of vertex trigger algorithms and to make more realistic tracking studies. We also plan to perform a study of pattern recognition issues in the RICH detector.

The BTeV electromagnetic calorimeter system will be used for triggering and observing $B \to e\nu X$ decays. In addition, the detection of photons and π^0's in BTeV is of great interest, though not necessarily an easy task. We plan to undertake a study of the BTeV electromagnetic calorimeter options so that we are able to develop a detector that will have the capability of measuring electrons, photons and perhaps π^0s coming from b-hadron decays.

Understanding the backgrounds levels in the detector will be an important part of the simulation effort. We need to have a thorough understanding of these backgrounds and their effect on the trigger and the various detector components. BTeV will work with physicists from the Fermilab Beams Division to undertake a comprehensive study of the beam related backgrounds inside the collision hall.

2.1.2 Simulation of Physics Processes

We have presented our understanding of the physics reach of BTeV for the measurement of B_s mixing and for the measurement of the angle γ. There are many additional measurements that will be part of the BTeV physics program. Several of these measurements are outlined in the BTeV EOI, including the expected sensitivity of the BTeV baseline detector for measuring the angles α and β of the unitarity triangle. In order to understand better the sensitivity to these modes, we plan to make more detailed studies of flavor tagging using the BTeV detector. We plan to continue a vigorous physics simulation program during the coming year in order to be able to make estimates of the sensitivity of BTeV for the following:

- Study of B_c decays
- Radiative B decays
- Searches for rare B decays
  - $B^o, B_s \to \mu^+\mu^-$
  - $B^\pm \to K^\pm\mu^+\mu^-$
  - $B^o \to K^{*o}\mu^+\mu^-$
  - $B_s \to \phi\mu^+\mu^-$
  - $B^o, B_s \to \mu e$
- CP asymmetry in $B_s \to J/\psi\phi$
- Charm physics (CP asymmetry, mixing, rare decays)

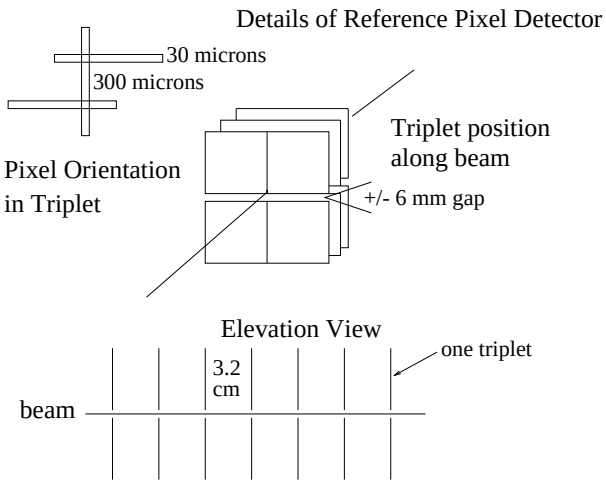

Figure 21: Layout of BTeV Pixel Vertex Detector

2.2 Pixel R&D plan

2.2.1 Introduction

The BTeV baseline vertex detector, shown in Fig. 21, has triplets of pixel planes distributed along the IR separated by about 3.2 cm. The individual planes are composed of four 5 cm × 5 cm quadrants, mounted above and below the beam so that a small vertical gap is left for the beams to pass through. In the present design, which is still being studied, we are considering pixels as small as 30 μm × 300 μm pixel and which feature analog read out of the charge collected by each pixel cell. Each triplet consists of one plane that has the short (high resolution) dimension oriented to measure the bend view, one that measures the non-bend view, and a third that measures the bend view again.

When compared to the other major pixel systems under development, the BTeV pixel detector has some unique features that should be noted: First, the pixel information will be used for the formation of the first level trigger decision. This implies that the read out has to be extremely fast and a self-triggering feature may be desirable. Second, the beam crossing interval at the Tevatron will be 132 ns which is considerably longer than that planned for the LHC. As a consequence, the front end electronics for the BTeV detector can be relatively slower than for the LHC pixel detectors with obvious benefits in power dissipation and in the general design of the analog front end. Third, the BTeV pixel detector will be operated in the vacuum and will be placed very close to the colliding beams. This places very stringent requirements on the radiation resistance of the detectors and their EM shielding from the beam induced disturbance.

The need for large pixel detectors at the LHC and elsewhere has generated a world-wide R&D effort and has led to rapid and steady progress and widespread collaboration. Fermilab has recently joined this global effort by establishing a pixel R&D group which is intended to address the needs of the next generation of high luminosity experiments at the Tevatron collider. BTeV members are participating in the work of this group which, by taking advantage of what has already been done, has made excellent progress. This bodes well for the success of the BTeV pixel R&D plan which we present here and which will take maximal advantage of the work being done elsewhere.

2.2.2 Plan

The BTeV pixel R&D plan is organized around five stages, each with increasing complexity. The stages are laid out roughly sequentially although they do partially overlap in time. Each stage has goals which are expected to be achievable on the time line anticipated, with other goals deferred to later stages. Thus, the plan is to arrive at the final system by a series of successive approximations of increasing sophistication and completeness. The lessons learned in meeting each stage will affect all later efforts.

In defining the detailed specifications for each stage, we will aim for the BTeV final performance goals wherever possible. Where it is not possible to go immediately to a final BTeV goal in one step, we will define intermediate steps which will move us toward the ultimate goal while allowing progress on other fronts.

Much of the work being done on pixel R&D by other groups is relevant to BTeV and we expect to take advantage of if whenever possible. As mentioned above, BTeV members are strongly involved in the Fermilab pixel effort, which in turn is trying to take maximum advantage of the work being done elsewhere. For example, progress has already been made on the first milestone listed below. Small chips of 30μm $\times$ 200μm pixels have been bump-bonded by two vendors. This success was achieved by the Fermilab pixel R&D group which includes some BTeV collaborators. It used a prototype read out chip that had been developed originally for the SSC. It also used sensors that were made specially for these tests by BNL. Some early results from this work are presented in Appendix A.

Below, in Table 4 is a list of the major 'stages', or time periods, planned for pixel R&D. Following that, for each stage, we discuss the main goals, include a list of specific milestones, and describe 'feeder' research, which will be done in each stage either to provide optional paths for that stage or to prepare for the work of subsequent stages. The program is planned around the idea that any delay in achieving a given goal at any stage does not destroy the possibility of meeting all the other goals at that stage. The feeder R&D tasks will be ongoing and will either be moved into the overall plan as they reach success and demonstrate their value or will be dropped. These feeder efforts include investigations of radiation hardness in the readout chip technology, detector and readout chip thinning, staggered bump bonding, and others.

By the time we reach stage 5, we are already dealing with a system that is quite large. It may not be appropriate to consider it as part of the R&D program but rather as the first step in 'production' for the full detector. We include it here to indicate the full path that we believe this project must take. Even the system planned for stage 4 is quite an ambitious one and might actually be larger in channel count than any existing pixel system with high speed readout. Substantial resources will be required to carry out stage 4.

Stage	Description	time span
1	Small chip assemblies	1997 to spring 1998
2	Multi-chip assemblies	1998 to late 1999
3	Module assemblies	mid 1999 to mid 2000
4	Full Station assembly	mid 2000 to mid 2001
5	Full BTeV System Prototype	end of 2000 to mid-2002

Table 4: BTeV Pixel R&D Main Development Stages or 'Time Frames'.

In addition, some members of BTeV will be participating in R&D into diamond pixel detectors as an option for BTeV. Diamond detectors have been shown to be about a factor of 100 more tolerant to radiation than silicon detectors. Diamond has excellent thermal conductivity and mechanical properties. These, coupled with the fact that diamond detectors have no leakage current, make diamond detectors a very attractive option for the innermost region where the radiation dosage is very high. Our simulation shows that there are some significant gains in resolution by moving the detectors closer to the beam. We have chosen the gap to be 6mm because of radiation damage to silicon (the electronics using rad-hard technology is expected to be at least ten times more tolerant than the silicon detectors to radiation). The use of diamond pixel detectors will enable us to operate the vertex detectors safely closer to the beam. We plan to carry out an R&D program on using diamond as sensor material for pixel detectors. Some members of BTeV are also members of the RD42 collaboration and this R&D will be carried out jointly betweeb BTeV and RD42.

Stage 1: Small chip assemblies: bump bonded readout chip and sensor – 1997 to spring 1998

The primary goal for this stage is to go through all the steps in design, fabrication and testing a small pixel detector. This means testing the read-out chip, design and fabrication of the sensor to match it, bump bonding, and testing the chip and the bump-bonded detector. A significant apsect of this work is to learn how to read out these detectors and to develop the expertise, equipment, and software infrastructure to carry out detailed tests on the their performance.

We are currently engaged in working towards this milestone and the results obtained so far are presented in Appendix A.

The milestones for this stage are:

1. Indium bump bond small readout chips to small sensor chips with pitches as small as 30 μm.;

2. Investigate the effect of coupling the sensor to the readout electronics – compare the performance of the read out electronics with and without the sensor substrate.

3. Bench test and beam test these detectors using infrastructure including equipment and computer programs developed for this R&D program.

4. Develop the design capability for the pixel readout chip.

Stage 2: Multi-chip assemblies – 1998 to late 1999

In this stage, the goal is to fabricate full chip assemblies. In particular, we want to make a system with two planes of chip assemblies of approximately 2 cm $\times$ 2 cm in area using a few prototype readout chips (with outer dimensions of order 1 cm $\times$ 1 cm) bump bonded to single sensor substrates. Most of the ideas and solutions we want to pursue for the full detector are already present here at a smaller scale. In this time frame, we will gain experience on system issues related to interconnect technology, minimizing material and dead area by building the detector system described above.

One important goal of this stage is to design the routing of the analog bias lines, ground and power supply lines, control signals, and data lines without increasing the noise or causing cross talk between different read out chips.

Another goal is to find the optimal way to match the sensor and the readout patterns so as to minimize material in the active area of the detector. This is a problem in any configuration having many readout chips on the same sensor. The region on the contour of the readout chips, between the actual end of the integrated circuit and the edge of the silicon chip, does not allow for a simple tiling scheme which covers the entire sensor substrate while keeping the pitch constant. We are currently investigating a solution, which should preserve at least the finer pixel segmentation, which is crucial for the BTeV trigger.

We hope that at the end of this stage we will have a full design for the read out electronics needed for BTeV.

The main milestones for this stage are:

1. Design a prototype readout chip that will meet the BTeV requirements

2. Begin to understand the issues associated with radiation hardened pixel sensors, which includes guard ring studies, leading to the possibility of running them at high voltage.

3. Multiple readout chips on a single detector

4. Chip to chip communication using single edge readout of devices

5. Readout chip dead space/overlap issues understood

6. Large scale reliability studies on bump bonding

7. Grounding and power supply distribution understood so that the intrinsic signal to noise of the detector can be maintained in the full system

8. Prototype cooling and support structures for a detector plane

9. Test of detector prototypes with beam in C0

10. Develop peripheral electronics including a control system to steer the hit information to the prototype trigger processor.

11. Understand possible EM disturbance from the beam and issues on RF shielding

In parallel, we will explore novel technologies such as multi-chip technology (MCM) that will allow for more efficient routing of the signals. Multi-chip technology uses the sensor chip itself as a substrate for routing the control signals and power. It would be possible to bump bond the chips to these lines and to the pixel cells of the sensor at the same time, with a dramatic simplification of the detector structure and

the fabrication process. We want to test on a real multi-chip structure the techniques we will adopt for the chip to chip communications and for those with the readout control circuit. If these studies succeed, we can fold it into the final design and implement it in the stage 3 system.

Another parallel effort is to develop a preliminary version of the cooling and support structure to get a better understanding of the approach to be taken to minimize the material introduced by these components in the active detector volume. Without careful optimization, the material of the support and cooling structures may be dominant contributors to the material budget. Some prototype cooling and support system will be required for the beam tests in C0 at this stage.

The effort on CVD diamond pixel sensors, mentioned above, will be going on during this period.

Stage 3: Module assemblies – mid 1999 to 2000

The goal of this milestone is to assemble and test a first prototype of the modules we will use as the building block of the whole BTeV pixel system. It will be the evolution of the prototype developed for stage 2 up to the full BTeV scale. It is clear that we will maximize the dimensions of the modules, compatible with the fabrication yield and the maximum achievable dimensions of the sensor substrate, in order to reduce as much as possible the number of overlaps among the modules required to form a single plane of the detector. One approach we are currently investigating is a linear array (ladder) of several pairs of readout chips, covering a sensor substrate area of about 2 cm $\times$ 5 cm or even 2 cm $\times$ 10 cm, if technically possible, to match the maximum dimension of the BTeV planes.

It is our intention to provide this prototype with the cooling system we will use for the final detector. Cooling considerations, in fact, deeply affect the structure of the modules and have to be taken into account, at least at some level, from early in the project. In our case, we are already evaluating the possibility of using a light thermoconductive layer made of beryllium, or of CVD diamond, that could serve as a mechanical support and a heat conductor at the same time.

At the middle of calendar year 2000, we will be ready to present a TDR for the pixel detector and can enter into the production phase whenever funds become available. Thus, the major goals of this stage of R&D are to have:

1. A final module assembly prototype (substrate, busses, grounding, etc.);
2. Possible first use of rad hard technology for the read out chip (although this might be deferred to the next stage);
3. A final design of the readout chip for BTeV including the trigger interface;
4. An optimized geometry of the system and the overall system configuration; and
5. Radiation tests of different components (read-out chip, bump-bonded detectors, and perhaps a full prototype module).

At this stage of the R&D program, it would be highly desirable to develop the module prototypes with radiation resistant components. This will be possible depending on the status of development of the readout chips and the sensors we are going to use. This should be viewed as 'feeder' research to stage 4.

Stage 4: Full Station assembly – mid 2000 to mid 2001

The goal here is to build a full station of three planes, to mount it in a small vacuum vessel with a realistic cooling scheme and alignment scheme and to try it out with beam in C0. This is the smallest scaleable building block of the full system and represents about 3% of the final system.

The milestones for this stage are:

1. Cooling;
2. Optimization of material budget and mechanical support;
3. Alignment; and
4. Full integration with trigger electronics.

Stage 5: Full BTeV System Prototype – end of 2000 to mid-2002

This phase is, in fact, the early part of the production. We would like to build a prototype of at least 3 stations which will be housed in something approximating the final vacuum and support structure and cooling system. We would like the vacuum vessel to be sized to hold the final detector so we could install dummy loads in the place of the missing active planes. The dummy loads would have the same weight and heat dissipation as the final detectors so many thermal, mechanical, and alignment issues could be studied. This 3 stations are about 10% of the full system but the large scale vacuum vessel prototype and the dummy loads should allow us to investigate many of the remaining problems at 'full scale'.

After studying the prototype performance and designing any modifications, we would be prepared to move ahead with full production as soon as the funding became available.

The milestones for this stage are:

1. Vacuum support;
2. Movable detector/readout relative to support; and
3. Power supplies, regulation, and voltage distribution.

Machine-Detector Interface and Mechanical Support

The development of the pixel sensors and the read out electronics, which we outlined above, are only part of the project to design a functional vertex detector for BTeV. The vertex resolution of this detector has been shown in Monte Carlo simulations to be highly sensitive to excess material. As such, emphasis will be placed on minimizing materials associated with mechanical supports and cooling to optimize vertex resolution. The close proximity of the pixel detector to the beam necessitates an RF shield for the pixel electronics [1]. In the past, this shield has also been used to separate the detector vacuum from the machine vacuum [2]. Furthermore, due to concerns about multiple scattering and secondary interactions, the amount of material to be used for shielding must be kept as low as possible. Innovative and unique solutions to these problems will be sought.

In order to study the severity of the RF pickup, we will work with Gerry Jackson, of the FNAL Beams Division and BTeV, to simulate beam conditions on a laboratory bench-top. A thin wire will be driven with an amplifier to simulate beam bunches. Surrounding the wire will be a prototype beam pipe compatible with BTeV pixel designs. An instrumented prototype detector will be used to study and map the RF pickup as a function of position with respect to the simulated beam. RF shielding designs will then be employed and tested within this beam simulator.

Due to variations in the beam position, the pixel detector must be withdrawn from the inner IR during Tevatron fills (about twice each day). A mechanical mover will be required to reposition the detector to an accuracy of better than 5 microns. Coupled with this mover will be cooling and mechanical support for the detector and electronics. Although no fundamental limitations are foreseen, the design will be technically challenging.

The shielding design will have significant impact on the overall IR and pixel design. As such, this work should be carried out as quickly as possible with the aim of having a workable shielding design by the end of 1998. Beam tests during 1999 in the C0 collision hall will be used to verify the results obtained from the beam simulator apparatus. Plans for building the beam simulator are well underway. Construction will begin within a few months with tabletop tests scheduled to begin by July 1998. Acceptable shielding solutions will be available by October 1998, with a preliminary RF shielding design completed by January 1, 1999. A prototype for testing will be fabricated and installed in the C0 collision hall by April 1, 1999, with a beam test to occur sometime during the 1999 accelerator program. Mechanical support and cooling designs will progress in parallel with the RF shielding studies. The goal is to have a working prototype ready for the C0 beam test in 1999.

2.2.3 Pixel R&D Organization

The development of the pixel detector is underway and involves the efforts of many groups and collaboration with industry and other experiments. A project organization is evolving to meet the demands of this project.

The pixel R&D project is divided into eight 'working subgroups' reporting to the project leader and covering the major activities now forseen for the project. Each working subgroup has a chairperson appointed by the project leader with the concurrence of the experiment's Executive Committee. It is the responsibility of the working subgroup chairpersons to report on the progress of their work to the project leader and to insure the successful and timely completion of the work assigned to the group in a cost effective manner. The responsibilities of the project leader and the manner in which the project will be reviewed are described above.

We are in the process of selecting chairpersons for each working group. The present composition of the working groups is:

1. Sensor R&D: what's needed for rad-hardened detector
   (D. Anderson, M. Artuso, D. Christian, K. Honscheid, H. Kagan, S. Kwan, J. Russ, M. Sheaff, C. White, A. Wolf)
2. Readout chip: electronic requirements, architecture, data-flow
   (J. Appel, E. Barsotti, A. Baumbaugh, G. Cancelo, D. Christian, J. Hoff, A. Mekkaoui, L. Moroni, S. Sala, W. Selove, S. Shapiro, R. Yarema, S. Zimmerman)
3. Bump Bonding: reliable, high yield, low-cost, fine pitch bonds
   (J. Appel, S. Kwan, J. Hoff)
4. Interconnect Technology: Multi-chip modules, control chip, HDI, flexi-circuit, ceramic PC
   (L. Moroni, S. Sala, S. Shapiro, M. Sheaff, S. Zimmerman)
5. Mechanical Mounts and Cooling: stability, material budget
   (R. Downing, C. White)
6. Simulation: study/optimize system configuration
   (M. Artuso, J. Butler, R. Kutschke, J. Russ, J. Wang)
7. Interface to Trigger/DAQ
   (E. Barsotti, A. Baumbaugh, J. Butler, G. Cancelo, D. Husby, D. Kaplan, W. Selove)
8. Beam Tests
   (Coordinator: D. Anderson)

2.2.4 Division of the efforts and interest of the groups

The current division of the efforts and responsibilities among the groups interested in the pixel development are shown below. It is based on the interest and the proven skill of the group in that particular area and the funds they may get from their funding agencies. Table 2 summarizes the interests and primary activities of the different groups on BTeV pixel R&D. We expect significant evolution of the roles discussed below as the BTeV project advances and as funding and manpower become available for the currently participating groups and for new institutions that will join the experiment.

- Carnegie Mellon University:

  The group is involved with BTeV R&D in several areas that impinge on the Pixel R&D program: (a) Readout Chip R&D; (b) Detector simulation and radiation damage studies; (c) Trigger/detector interface; CMU has people actively participating in all three areas now and expects to maintain and expand that activity over the next three years.

- Fermilab:

  The group will work on the design, development, and testing of the read out chip for BTeV, will carry out bump bonding studies and studies on radiation-hard silicon sensors, and will work on the interface between the trigger and the DAQ.

- Illinois Institute of Technology:

  The IIT group intends to study the infrastructure requirements of a pixel detector for BTeV, including mechanical support, cooling, and RF shielding. The group will also function as a liaison between the beams division and the BTeV pixel group. Some effort will be put into developing radiation hard alternatives to silicon. The Illinois Institute of Technology possesses a highly capable mechanical engineering department, and collaboration with this department throughout the design phase is expected.

- INFN-Milano:

  This group intends to take an active role in the development of the techniques for the interconnections of the pixel system. They will investigate the possibilities offered by the new technologies, such as MCM, to simplify the detector structure and, as final goal, reduce the amount of passive material embedded into the system.

  Further commitments will be considered by them depending on the evolution of the Italian participation in BTeV.

- Ohio State University:

  The group plans to be involved in sensor R&D in the area of radiation hardness. The group is especially interested in developing the diamond pixel option and has been an active participant in RD42 at CERN for several years.

- University of Pennsylvania:

  This group is studying the factors affecting optimum pixel dimensions, and the feasibility of readout-chip designs which would have minimum dead area. These studies are intimately coupled to questions of readout speed, feasibility of analog output, and the design of the readout system which will connect individual chip outputs to the driver which sends pixel information off the vertex detector.

- Syracuse University:

  Initially, they will focus on the sensor design, identifying the geometrical parameters for optimum physics performance and the technological issues involved in having a reliable and radiation hard sensor. In particular, for a n+ on n type sensor in the final detector, they will investigate the optimal design and identify the vendors interested in producing the detectors.

  They are also interested in pursuing technologies that would allow to route control signals and analog bias either on the detector hybrid structure (similar to the one investigated by CERN-Wupperthal in collaboration with IMEC) or on the cooling substrate. They will also study submicron CMOS process for readout chip design.

- Wisconsin:

  This group will ask for access to the Wisconsin Center for Advanced Microelectronics to perform research on pixelated silicon sensors for BTeV. They will also perform simulations of the processing and of the resulting electrical properties of the sensors.

Group	*Primary Tasks*
CMU	*Readout, Sensor, Simulation*
Fermilab	*Readout, Sensor, Bump bonding, Mechanical, Cooling, Simulation*
IIT	*Detector/machine interface, Mechanical*
Milano	*Interconnect, Multi − chip module*
OSU	*Sensor development, Simulation*
UPenn	*Readout, Simulation*
Syracuse	*Sensor, Simulation, Interconnect, Readout*
Wisconsin	*sensor, Interconnect*

Table 5: Groups and Primary Responsibilities for the BTeV Pixel R&D

2.2.5 Budget

Table 6 summarizes the funding request from the various groups on pixel R&D. Note that the Fermilab figure comes from three different groups and is for developing in-house capability to design, build and operate pixel systems for Tevatron experiments including BTeV.

Group	*FY*98	*FY*99	Fund Source
CMU	10*K*	10*K*	NSF
Fermilab	320*K*	670*K*	FNAL/DOE
IIT	25*K*	25*K*	NSF
Milano	100*K*	100*K*	INFN
OSU	22*K*	15*K*	NSF
Syracuse	81*K*	88*K*	NSF

Table 6: Funding request for the BTeV Pixel R&D. The Fermilab budget comes from three different groups: Radiation Hard Vertex Detector R&D group, Electrical Support Team from the Particle Physics Division, and the Electronic System Engineering Department in the Computing Division and is for all pixel related R&D activities at Fermilab. The Fermilab budget for FY98 is the currently allocated amount. The original request was $440K. The number for FY99 has the status of a budget request. The other institutions are in the process of requesting funds. We show the amount of proposed requests and the proposed funding source(s).

References

[1] "Grounding and Shielding in the Accelerator Environment", Q. Kerns, 1991 Accelerator Instrumentation Workshop, CEBAF, Newport News, Virginia October 28-31, 1991.

[2] J. Ellett *et al.*, NIM **A**317 (1992) 28-46.

2.3 Trigger and Data Acquisition System R&D plan

The BTeV trigger system must be capable of inspecting every beam crossing, without incurring any loss of data from deadtime, and must retain events which permit the widest possible investigation of the decays of b and c quarks. The experiment is designed for a bunch crossing interval of 132 ns and an initial luminosity of $5 \times 10^{31}\,\mathrm{cm}^{-2}\mathrm{s}^{-1}$ with the expectation that the luminosity will eventually be increased to 2×10^{32} or higher. The interaction rate at 5×10^{31} is 3.5 MHz and the B rate is about 5 kHz. The geometric acceptance of the BTeV detector is about 20%.

We believe that the physics topics that need to be addressed in the second generation B experiments will require studies of many decay modes, including all-hadronic modes. Although hadronic decay modes can be accumulated by triggering on dileptons or even single leptons, these collection methods are very inefficient, even when the lepton is used a flavor tag, because leptons represent only about a tenth of the useful flavor tagging efficiency. To achieve high efficiency, BTeV plans to use a secondary vertex or impact parameter trigger at the first trigger level, which we call "Level I." By triggering on the basic property of B decays, the presence of secondary vertices, BTeV hopes to achieve high efficiency and low bias which will enable it to do a broad range of precision studies.

In order to achieve this ambitious goal, BTeV must use the most modern and most cost-effective electronics and computing technologies. We also need to develop very efficient algorithms so that the total number of CPU cycles can be kept to a reasonable level. This requires the trigger design to be closely coupled to the pixel vertex detector design because the trigger will work best if the tracking system is arranged to facilitate the trigger calculations. Also, the trigger must be proven to be robust against many real world effects such as noise, multiple interactions, photon conversions, hadronic interactions, machine background. Finally, even with an excellent trigger, it is likely that BTeV will need to record on permanent storage of order hundreds to one thousand events per second. The current status of the Level I vertex/impact parameter trigger simulation is described above. We also plan to have muon and electron triggers at Level I. After Level I, there will higher levels of trigger selection which will have available to them all of the data from the whole event including the data from the forward tracker. We need to develop the algorithms for these higher levels and the architecture for the whole trigger system and DAQ.

To realize this project, it will be necessary to do R&D in several areas. The Trigger and Data Acquisition (TRIDAS) R&D for BTeV for the next two years will include at least the following activities:

1. Level I algorithm development;
2. Level I hardware architecture and prototype development;
3. Vertex trigger/tracker interface;
4. Level I muon system development;
5. Level I electron trigger development;
6. Global Level I trigger design;
7. Higher level trigger architecture and algorithm development;
8. DAQ architecture design; and
9. System simulation.

Since technology is changing rapidly, BTeV's strategy is to establish first that a viable trigger algorithm can be developed and implemented with today's hardware. We are proceeding by doing as much as possible using physics and electronics simulations. In addition, small scale prototypes need to be developed so that tests can be done to choose the most suitable electronic parts (FPGA's, microprocessors, high speed switches, etc.). We need to verify that the speeds and throughput required of the system can be achieved. The actual construction of a large-scale system should be deferred to the last possible minute, since technology will be improving and costs will be dropping with time.

Our understanding of the trigger performance is only as good as the simulation which makes certain assumptions about the performance of the detector elements and about the background environment. The

simulation effort must establish an "envelope" of performance and background parameters within which the trigger can operate successfully. Hopefully there will be a large margin between the expected operating point and the edges of the envelope. It will be necessary to check the performance of all the detectors involved in the trigger, all the trigger components, and all the noise and background assumptions as soon as possible to make sure that they stay within the boundaries of the envelope.

The data acquisition system, starting with the front end, relies on massive buffering of data while the trigger system makes a decision. The trigger pipeline can be many events long if the event size is sufficiently small. Early sparsification may thus be a key feature of the system. The trade off between more and better processors and more buffer memory needs to be understood.

Finally, the upper section of the trigger system will consist of farms of commercial processors. One important task of this part of the trigger will be to reduce the amount of data per event that needs to be archived. Ideally, one would like to write essentially a DST-like event to archive but this will come only after the detector is very well understood and automated alignment and calibration techniques are established. Developing a realistic understanding of the amount of data that might need to be handled at each stage and a strategy for dealing with it is an important component of trigger and DAQ R&D.

2.3.1 Level I Vertex Trigger Algorithm development

This includes simulations of various trigger algorithms based on a variety of possible tracking systems. We are especially determined to develop an integrated trigger-tracking system which is optimized for doing detached vertex triggering.

Our goal is to have a final algorithm or set of algorithms within the next two years.

Some key tasks in algorithm development are:

1. Continue to explore the baseline algorithm. This includes
   (a) Making the input data to the trigger simulation as realistic as possible. It must include accurate descriptions of electronics performance, physics processes, machine backgrounds, and noise. A full GEANT simulation as well as additional work with MCFAST will be required.
   (b) Exploration of other options within the context of the baseline approach. This includes assembling "secondary" tracks into vertices, forming masses at vertices, etc.
   (c) Optimization of the calculations for various classes of processors.
2. Develop fully at least one additional algorithm based on a different distribution of pixel planes along the IR. We are already investigating a scheme based on doublets (rather than triplets) at each tracking station. We may also evaluate a scheme where the pixel planes are simply evenly spaced along the IR.
3. Exploration of algorithms that use track information from the vertex processor to make selections based on event topology or kinematic quantities other than impact parameter or multiple vertices – for example, the total P_t of the charged tracks. These algorithms may be very useful for charm triggers.
4. Evaluate the possibility of using downstream tracking to provide improved momentum information at Level I.
5. Evaluate the use of other detection elements such as drift or proportional chambers looking at wide-angle tracks to help localize the primary vertex in the Level I trigger.

2.3.2 Level I hardware architecture and prototype development

This task involves the construction of prototype hardware for the trigger and investigations of its performance. For the reasons mentioned above, the prototype will be on a fairly small scale – probably amounting to one or at most a few of the basic parallel units of the trigger.

The prototype will serve 3 purposes:

- As a testbed to develop and test algorithms for hit finding, track finding, and vertex finding. This will help us understand the processing requirements for each trigger stage, uncovering bottlenecks and latency problems. It will allow software to be tested in a realistic environment that addresses issues

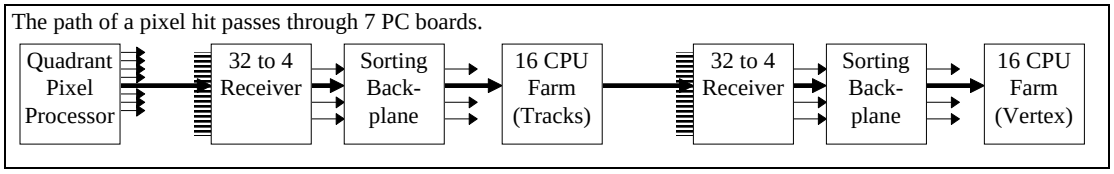

Figure 22: Flow of pixel hit through trigger system

such as data movement, memory limitations, and operating-system interface. Simulation is insufficient for this task because data movement and formatting take a significant part of the processing time and are highly dependent on the hardware implementation.

- Test data flow in real time using simulated data. The trigger system relies on small FIFOs in each data path to smooth out the differences between peak and average data rates. This architecture allows for efficient use of resources, but it is somewhat susceptible to large bursts of "non-average" data. The prototype will allow us to optimize data flow and understand exceptional conditions.

- Create an infrastructure that will allow us to move from prototype to final system with little additional work. Circuits and software developed and debugged in the prototype can be used with very little modification in the full trigger system.

The baseline vertex trigger system consists of 340 circuit boards of four different types. Data from a single hit pixel will pass through seven of these boards on their way from the pixel detector to the trigger output. This flow is shown in Fig. 22. The prototype will be a single circuit board that contains all of the switching and processing elements to test the entire data path at full speed.

The prototype board will contain four hit processors, four track/vertex processors, and associated data paths. The data paths are implemented in FPGAs, so their configuration can be varied to test different sections of the trigger. For example, when testing the hit-to-track data flow, the switching elements will operate on 64-bit words. When testing the track-to-vertex path, they will operate on 128-bit words. Large FIFOs will be used to buffer the incoming test data and to capture output data. Data path usage will be monitored in real time, allowing a graphical representation of data flow for all data paths. All control and monitoring of the prototype will be done via a Windows-NT PC host. A schematic of the board is shown in Fig. 23.

The approach used for algorithm evaluation will be to deposit simulated pixel hits in the input FIFO and process them using the prototype trigger hardware. Actual timings for the trigger codes can then be studied and optimized. We believe hardware tests will be an economical and efficacious and will also move us efficiently along the path to actual implementation. We may also want to carry out a detailed low-level simulation to aid in designing and optimizing the final hardware.

The prototype effort consists of the following major tasks:

1. Seven major FPGA designs with 1 to 4 variations on each. Each design represents from one to four man-months of effort which should be transferable with relatively minor changes to the final system design. These include two high speed microprocessor interfaces, with considerable design effort dedicated to balancing processing work between FPGA circuitry and microprocessor software. Other FPGA designs include a merge chip, a sorting switch, a buffer manager, a host interface chip, and a datapath monitor chip.

2. Operating system design, which includes interfacing application-level software to the hardware and the host. In addition to low level operating system software on each type of microprocessor, this includes design of a large scale hosting system. In the final system, there will be 6,000 to 19,000 programmable devices, including ~3,000 FPGAs and ~3,000 microprocessors, and perhaps including pixel chips which represent an additional 13,000 devices which must be programmed to some extent. The host system is designed to handle bit stream configuration for this large number of devices as well as downloading software and monitoring of device status. This represents about 6 months of effort which will be transferred from the prototype to the final system.

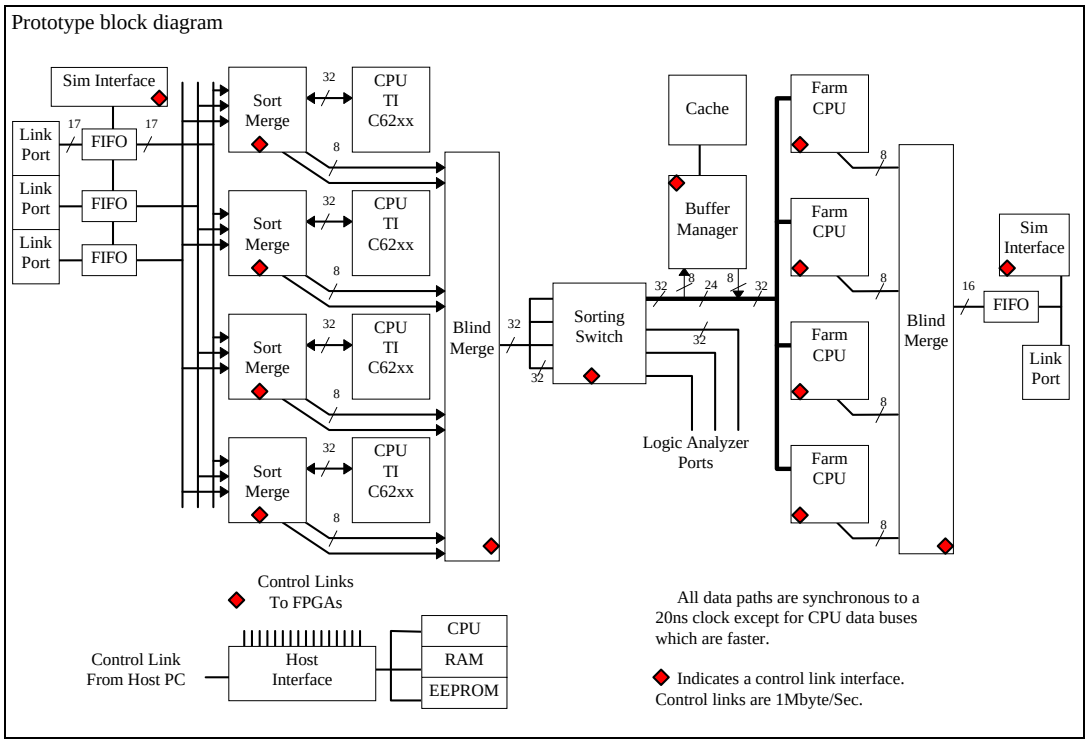

Figure 23: Schematic of prototype trigger board

3. Board-level design, including circuit board layout, power distribution, clock distribution, and cooling, which represents 2-4 months of effort.

4. Creating development environments for users, including gathering tools and documentation for each type of microprocessor and programmable device in the system. This represents about 1 month of writing documentation and 1 month of installing and learning how to use compilers and assemblers.

5. Application software development. This includes algorithm development and porting and optimizing of existing algorithms.

Hardware design for the prototype is currently in progress. Circuit board layout is about to begin and assembly should be done in the Spring of 1998. Software development can begin in January of 1998.

2.3.3 Vertex trigger/tracker interface

This activity involves doing technology studies to determine the best way to move data into the first level trigger and, if indicated, to build prototype hardware to validate the proposed technology.

2.3.4 Level I Muon system development

The muon trigger is intended to provide an alternative trigger path for events which contain signal or perhaps tagging muons. It will surely have a dimuon capability and single muon capability will be investigated. It should be capable of operating independently of the vertex trigger or in conjunction with it. The goal is to design a "stand-alone" trigger which uses the muon chambers to make a crude measurement of the muon momentum which is then used to compute a dimuon invariant mass. This system would provide an excellent calibration of the performance of the vertex trigger algorithm. The "OR" of the two triggers results in very high efficiency for states with dimuons from B's in the spectrometer acceptance. The system will also be capable of providing the P_t of single muons which could be used in conjunction with the vertex detector (with loosened requirements) to improve the efficiency for states with single muons.

The project includes the formation of trigger primitives and their processing to form a Level I trigger in a time well below that of the vertex trigger.

The major effort for the next year will be to develop a design for a muon system that will facilitate the formation of these kinds of triggers. In addition, a hardware effort using FPGA's is being initiated to understand how such a trigger might be realized.

A parallel effort will be to evaluate the effect of hadronic punch-through and decay in flight on the muon detector and especially the trigger. Also, muon triggers have frequently suffered badly from the presence of beam-related background or particles spraying off of collimators. This has been especially true for muon detectors in the forward rapidity region covered by BTeV. The muon group intends to develop a rather detailed simulation of the particle backgrounds with the assistance of experts from the Fermilab Beams Division. The muon trigger group will participate in this effort since the trigger is very vulnerable to these backgrounds.

2.3.5 Level I electron trigger development

This has a function which is very similar to that of the muon trigger. However, the design of the electron identification system is not very far along and is connected to the issue of how well we can do on photons and π^o reconstruction. Serious work in this area will need to wait for a more complete design of the electron and photon detector.

2.3.6 Global Level I Trigger

The Level I trigger has several components which must be formed into a single global trigger. We expect to have one or more main physics triggers, which will come from the vertex trigger, and which will not be prescaled even at the highest luminosities. Other physics triggers and partial triggers (with some requirements relaxed to calibrate the main triggers) may run at higher rates and might need to be prescaled at the highest luminosities. The global Level I trigger needs to synchronize decisions coming from the various components, needs to provide the ability to prescale the various subtriggers, and needs to provide diagnostic signals so that the rates of all key trigger components can be carefully monitored.

The group doing this task will be responsible for the hardware of the global Level I trigger. It will also be responsible for tracking the estimated trigger rates for each trigger component and, if necessary, assigning target "bandwidth allocations" to each.

For the next two years, the task will involve assembling the list of proposed triggers, setting up the framework for tracking the rate estimates as they evolve, and beginning the process of setting the bandwidth available to each one.

2.3.7 Higher level trigger architecture and algorithms

It is well understood that there will need to be additional computations beyond what we have considered so far in Level I. These will use more of the data from the whole event. The vertex tracker and forward tracker will certainly be used together in these steps. Improved measurements of the momentum will allow one to tighten impact parameter and vertex cuts and to use the invariant mass at the secondary vertex to select B decays. It is also expected that the ability to reject events with multiple interactions, a small fraction of which may fool the trigger, can be improved in these higher trigger levels. The architecture of this system must be designed and the algorithms it will run must be developed.

2.3.8 DAQ architecture

The event building, buffering, and recording scheme which moves the data onto an archival medium needs to be designed. It is very important to get an accurate idea of how much data must be moved and stored at each stage of the triggering and data acquisition process. This group will estimate, using simulation of detector occupancies and whatever can be learned concerning detector noise performance and background, the amount of data that will be input to each level of the trigger and the amount of data that must be buffered at each level. It must develop a strategy for reducing the amount of data that must be recorded on a permanent medium. It must consider the data path and rate from the last level of the trigger to the archival storage system. It must consider the architecture of the archival system and must take into account

the cost of recording media and the problems of data retrieval. The group must also consider issues such as clock distribution, slow control, calibration and monitoring, and hardware configuration needs.

2.3.9 System simulation

This task includes simulating the system including front end buffering/storage, transport to Level I processors and buffering, Level I execution time, transport to higher trigger levels, and eventual archiving. The simulation must help determine the depth of buffering, pipeline lengths, and possible bottlenecks or sources of deadtime throughout the whole system.

In the next year, we will probably review commercial tools for carrying out this program. However, we will not commit significant resources to it until we understand how much information we can derive from our hardware prototype. It may be that we can learn enough from the hardware prototype so that the system simulation can be done at a fairly high level mainly to check whether performance observed in the prototype will scale or hit bottlenecks at the higher levels of the trigger.

2.3.10 Institutional commitments

- Carnegie-Mellon University:

  CMU is working on item 1 (Level I Algorithm development). They are currently investigating schemes that can use fewer pixel planes (2 per station) and suffer lower efficiency losses than the baseline proposal. This scheme would involve more computation and data movement. This work is being done chiefly by Alek Kulyatsev with direction from Mike Procario. CMU plans to move into items 2 and 3 (Level I hardware architecture and prototype development and Vertex trigger/tracker interface) when their algorithm work matures. This area interfaces with the other CMU work on the vertex detector. CMU is planning to expand its involvement to include work on items 7, 8, 9 (Higher level trigger architecture and algorithms, DAQ architecture, System simulation).

- Illinois Institute of Technology:

  The IIT group will work on items 1, 2, and 3. They are strongly interested in optimizing the vertex trigger for charm. They will request another postdoc from DOE in our next renewal (starts April '98) who could work on this. If more resources are available to them, they would consider participating in the trigger prototype.

  The IIT group also intends to investigate architectures for high-speed massively-parallel event building and distribution. Such a system is a necessary component of the BTeV TRIDAS system and could be utilized at Level 1, 2 or 3, depending on what architecture is chosen for these systems following prototype studies and further architecture and algorithm evaluation. They propose a modest prototyping and evaluation effort aimed at producing a system consisting of a few circuit boards to demonstrate the approach and evaluate potential bottlenecks in the dataflow and control.

- Fermilab:

  Fermilab plans to continue to evaluate and refine the algorithm for the baseline vertex trigger design. It also plans to work to make the simulation more realistic by adding other sources of background and studying multiple interactions.

  Don Husby of Fermilab is in charge of the trigger prototype project. The Fermilab group plans to assign at least one person to work with Don Husby on the hardware simulation package.

- University of Pavia:

  Pavia is involved in the hardware design of the level 1 muon trigger system with 3 researchers. The proposed R&D was approved by INFN on a time range of two years. For the first year (1998) they will have about 17 K$ in order to buy the PGA development-system package and to start the development of the PGA internal programming. At the moment they are working on the logic combinations of the muon detector signals in order to learn how much PGA microcircuits are needed.

Group	*Primary Tasks*
CMU	Level I trigger algorithm development, pixel detector/trigger interface higher level triggers
Fermilab	Level I trigger simulation and trigger prototype, overall architecture
IIT	Simulation for charm trigger, event builder prototype
Pavia	Muon trigger electronics
U of Illinois	Muon system layout and trigger simulation
U of Minnesota	Trigger simulation
UPenn	Trigger simulation and pixel detector/trigger interface

Table 7: Groups and Primary Responsibilities for the BTeV Trigger R&D

Group	FY98	FY99	Source
Fermilab	33K	33K	FNAL/DOE
IIT	20K	30K	NSF
U of Minnesota	13K	3K	NSF
Pavia	17K	17K	INFN

Table 8: Funding Requests for BTeV Trigger R&D

- University of Illinois:

  Jim Wiss is presently working on optimizing the overall layout of the BTeV muon system, epsecially as concerns the trigger. This activity is primarily concerned with the ability of the muon system to provide a stand alone mass or P_t trigger.

  After these conceptual design studies are brought to a successful conclusion, they will study the effects of noise hits and punch-through due to hadronic showering in the E&M calorimeter. Such additional "noise" is likely to influence the effectiveness of possible muon triggers and/or muon off line muon identification efficiency and miss-identification rate. These studies will undoubtedly influence the trigger design and may influence decisions concerning the amount of readout redundancy required for an adequate trigger. At present, they are planning the use GEANT Monte Carlos in conjunction with McFast to model hadronic shower debris and muons from pion and kaon decay.

- University of Minnesota:

  Profs Kubota and Poling along with a postdoc and student plan to work on the trigger algorithm development. Their interest is in studying trigger performance of various hardware pixel configurations as well as "software" or algorithms. Trigger performance will be measured using one or two bench-mark physics topics such as B_s mixing.

- University of Pennsylvania:

  They will continue to work on refining the trigger capability, improving the algorithms both for primary vertex finding and for triggering. This work involves, among other things, optimizing the pixel dimensions particularly for small angle tracks of relatively high P_t, which are especially important for improving trigger efficiency and reducing background. These steps are particularly important both for charm physics and for flavor tagging by tracks which clearly miss the primary vertex. This group will also work on the interface design between the pixel chips and the trigger processor as a natural extension of its work in the pixel group.

2.3.11 Responsibilities and Budgets

The current distribution of responsibilities is given in Table 7.

The current budget requests of the groups participating in trigger and data acquisition system R&D is:

Fermilab plans to construct the small scale Level I vertex trigger test bed with the requested funds. The first year is budgeted and the second year funding will be requested. Pavia has an approval for funding for

two years for R&D on the muon trigger. The IIT budget request is for technical support and material and supplies to construct a small scale prototype event building system. The Minnesota budget request is for $10K in the first year for 3 Aspen computers 533 MHz, 9 GB disk each. They also ask for $3K a year for travel to Fermilab for consultation with BTeV collaborators and to attend BTeV meetings. University of Illinois' efforts on the muon trigger are supported under Muon System R&D since they are closely tied to the detector design (see below). CMU and University of Pennsylvania are preparing funding requests.

References

[1] M. Bowden *et al.*, "A High-Throughput Data Acquisition Architecture Based on Serial Interconnects," IEEE Nuclear Science Symp., Orlando, FL, 1989.

[2] D. Black *et al.*, "Results from a Data Acquisition System Prototype Project Using a Switch Based Event Builder," IEEE Nuclear Science Symp., Santa Fe, NM, 1991.

2.4 Muon System R&D plan

The BTeV muon system has two primary functions:

- B Physics Involving Muons: Many of the experiment's physics goals (rare decay searches, CP violation studies which require tagging, studies of beauty mixing, searches for charm mixing, etc.) rely on efficient muon identification with excellent background rejection.
- J/ψ and Prompt Muon Trigger: Besides providing interesting physics, this trigger performs an important service role by selecting (bottom) events on which the more aggressive and technically challenging triggers (such as the vertex trigger) can be debugged and evaluated.

In designing a system that serves the above purposes it is important to understand the backgrounds from the accelerator, interaction point, and hadronic showers in the EM calorimeter. Such an understanding is critical in light of the fact that the rapidity coverage of the system is significantly more forward than for previous collider detectors.

In order to produce an initial design of the muon system there are several issues that need immediate attention: choosing detector technology and front-end electronics, "environmental studies" (backgrounds from the interaction point and the accelerator), geometry optimization, trigger optimization, and trigger electronics research and development.

2.4.1 Detector and Front-end Studies

The detector technology selected must be robust, have a high rate capability, have good time (30-40ns) and spatial (2-3mm) resolution, and have minimal neutron susceptability. We believe that proportional tubes are the most cost effective and conservative technology consistent with the above criteria, but there are several studies we need to make to prove that this is so. There has recently been significant work by other collider groups on new fast gases, and we would like to investigate the suitability of these to our application. We would like to make aging studies, investigate the possible problem of neutron activation, and determine the drift velocity, efficiency, rate capability and noise for different tube geometries. We intend to run the tubes in proportionl mode. While this requires amplification, it will help significantly with robustness, aging, rate capability, and noise. We would therefore like to evaluate and test front-end electronics such as the Penn ASD (amplifier–shaper–discriminator) chip. We intend to set up a test stand to perform these studies, and if we get sufficiently far along hope to perform some beam tests. If we feel they are necessary, we may try to perform neutron activation studies. (A test-stand has been set up at Karlsruhe for this purpose, and has been used by the CMS collaboration.)

2.4.2 Environmental Studies

There are several Monte Carlo studies of importance for understanding the backgrounds in the muon system. We would use these simulations to study the the effect of backgrounds on trigger strategies and on muon identification algorithms.

In order to achieve adequate momentum resolution for triggering, we would like to measure muon trajectories both upstream and downstream of the magnetic toriod. We are concerned about whether the upstream chambers can be adequately shielded against hadronic showers which originate in the electromagnetic calorimeter. Geant-based Monte Carlo simulations are required to study the effect of leakage from the calorimeter. Other sources of "interaction-point" backgrounds such as decays in flight need to be included in these studies.

The "gas" of neutrons and other particles that accompanies the beam needs to be understood. N. Mokhov and S. Droshdin in the Beams Division at Fermilab have developed code (such as MARS) which can be used to make these studies, and have used this code for applications at LHC and the Tevatron. Such studies can be useful both to design adequate shielding and also for calculating expected noise rates from accelerator based backgrounds.

2.4.3 Geometry Optimization

More detailed Monte Carlo studies than those described in the BTeV EOI, in conjunction with the environmental studies above, need to be performed in order to optimize the geometry of the system (number, location and resolution of the detector elements).

2.4.4 Trigger Strategies

Detailed Monte Carlo Studies of the efficiency and rejection of various trigger strategies need to be made. These are discussed in the Trigger R&D section.

2.4.5 Trigger Electronics R&D

Research and development work for the muon trigger electronics is underway at Pavia, and has been funded by the INFN. These are discussed in the Trigger R&D section.

2.4.6 Budget Request

Out total request is for $50,000 in each of the next two years. This will be used for computing hardware, technical support personnel, materials and supplies needed for detector development. It does not include overhead. These funds will support the efforts described above, which will be performed by the Illinois, Puerto Rico, and Vanderbilt groups in BTeV.

- Computing: significant MC studies, as described above, are required. Hadron shower simulation and background rejection studies require large amounts of CPU time and the ability to store large event samples. At the present time the computing resources we have available to us are being devoted to analysis of data from our current experiments. In the first year, we request two workstations and some large disk drives ($20,000). This money will be split between the Illinois and Puerto Rico groups.
- Materials: materials, gas, radioactive sources, etc., needed for construction and testing of detector prototypes ($15,000 each year). These funds will go to Vanderbilt.
- Technical support for detector design and development. ($15,000 the first year, $20,000 the second). These funds will go for hourly wages for technical support personnel who assist in the design of the BTeV muon system, detector development work, and the development of the hardware that will be used in the construction of the final muon system. These funds will be split evenly between Illinois, Puerto Rico, and Vanderbilt.
- Supplies and materials needed for the develoment and fabrication of the hardware needed to construct the final system (wiring jigs, etc.). These funds ($15,000 in the second year) will be split evenly between the Illinois, Puerto Rico, and Vanderbilt groups.

Table 9: Budget Summary: Muon R&D

Item	Vanderbilt	U of Illinois	U of Puerto Rico
First Year Funding:			
Computing		10.0K	10.0K
Materials support for proto-development	15.0K		
Technical Support	5.0K	5.0K	5.0K
Materials & supplies prototype construction			
Total	20.0K	15.0K	15.0K
Second Year Funding:			
Computing			
Materials support for proto-development	15.0K		
Technical Support	6.6K	6.7K	6.7K
Materials & supplies prototype construction	5.0K	5.0K	5.0K
Total	26.6K	11.7K	11.7K

2.5 Charged Hadron Identification R&D Plan

Excellent charged hadron particle identification is a critical component of a heavy quark experiment. In the design of any particle identification system, the dominant consideration is the momentum range over which efficient separation of the various charged hadron types – π, K, and p – must be provided. In BTeV, the physics goal which sets the upper end of the momentum requirement is the desire to cleanly separate $B_d^o \to \pi^+\pi^-$ from $B_d^o \to K^+\pi^-$ and $B_s^o \to K^+K^-$. Fig. 24a shows the momentum distribution of pions from the decay $B_d^o \to \pi^+\pi^-$ mentioned above for the case where the two particles are within the spectrometer's acceptance. The low momentum requirement is defined by having high efficiency for 'tagging' kaons from generic B decays. Since these kaons come mainly from daughter D-mesons in multi-body final state B-decays, they typically have much lower momentum than the particles in two body decays. Fig. 24b shows the momentum distribution of 'tagging' kaons for the case where the signal particles are within the geometric acceptance of the spectrometer and exit the the end of the spectrometer dipole. Based on these plots, we have set the momentum range requirement for the particle identification system to be: $3\,\mathrm{GeV/c} < P_{particle\ id} <\sim 70\,\mathrm{GeV/c}$. Kaons and pions from directly produced charm decays have momenta which are not very different from the kaons from B-decays.

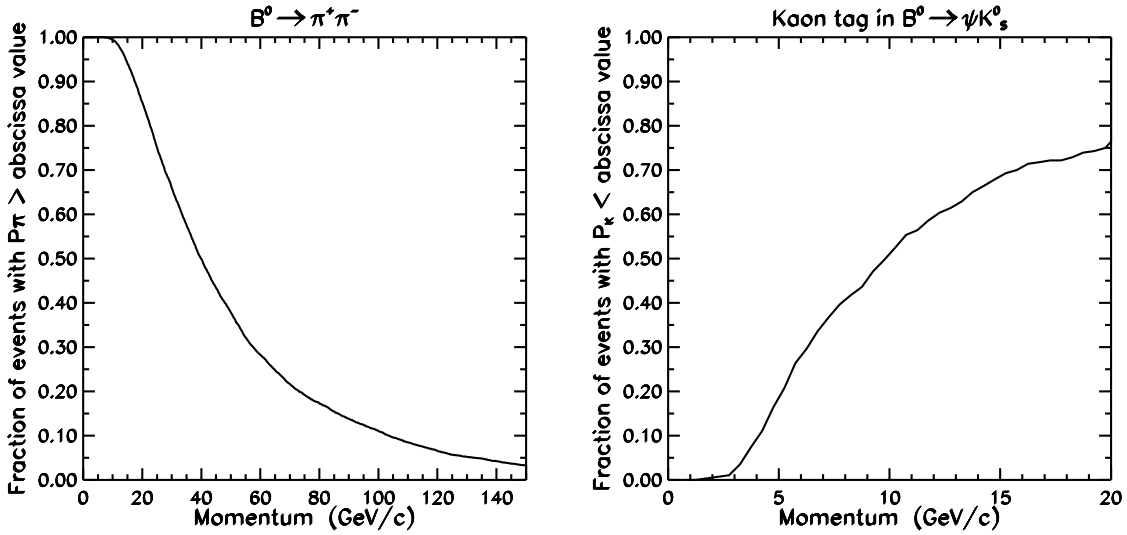

Figure 24: (a) On the left: loss of efficiency for $B_d \to \pi^+\pi^-$ as a function of the high momentum cut-off of the particle ID device. (b) On the right: loss of kaon tagging efficiency for $B_d \to \psi K_S^0$ as a function of the low momentum cut-off of the particle ID device.

Because of the large momentum range and limited longitudinal space available for a particle identification system in the C0 enclosure, there is really only one choice of detector technology – a gaseous ring-imaging Cherenkov counter. Fortunately, there are gas radiators which provide signal separation between pions and kaons in this momentum region. Two candidate radiator gases, C_4F_{10} and C_5F_{12}, have $\pi/\ K/\ p$ momentum thresholds around 2.5/ 9.0/ 17.0 GeV/c respectively. C_5F_{12} was used in the barrel part of the DELPHI RICH [1]. It needs to be operated at 40°C because of its high condensation point. The C_4F_{10} gas can be used at room temperature. It was used in the DELPHI endcap RICH and was adopted for the HERA-B [2] and LHC-B RICH detectors [3].

The size of the central dipole magnet and the longitudinal space available constrain the radiator thickness to $1 - 3$m and mirror radius to $5 - 7$m. To place the photo-detection plane outside the flux of charged particle exiting the magnet, the mirror must be tilted. If the radiator is too short, the tilt angle becomes large enough to dominate Cherenkov angle resolution. Therefore, the longer radiators and the larger mirror radii are preferred. This will also maximize the photo-electron yield from the gas radiator. Because of the open geometry of the forward spectrometer and the absence of magnetic field around the PID device,

Cherenkov photons can be detected by an array of photo-multipliers. The R5900-M64 multi-anode tube recently developed by Hamamatsu has a sufficiently small anode size not to effect Cherenkov angle resolution. Detection of the Cherenkov spectrum in visible wavelengths allows the use of inexpensive window materials, standard photo-cathodes and a simple gas system. Fast response, large gain and durability are the other advantages of the PM system. The Multi-anode photo-tubes R5900-M16 were adopted for the HERA-B RICH detector (the mirror radius is about 11m in HERA-B allowing for coarser segmentation). Hybrid Photo-Diodes offer an alternative photo-detection scheme. The upstream LHC-B RICH detector has a small mirror radius (2m), and thus requires a smaller photo-detection cell size than needed in BTeV and that is provided by the multi-anode tubes presently available. Therefore, the LHC-B collaboration is pursing an R&D program to develop HPD read-out.

Simulation and prototyping work is needed to work out details of the RICH design: radiator length, mirror tilt, location of the photo-detection surface, light focusing (if any) to avoid dead areas of the photo-detectors, optimal segmentation, window and photo-cathode materials etc., and to choose between the PM and HPD systems.

Even though a single gas radiator like C_4F_{10} can provide π/K separation in a sufficiently large momentum range ($3-70$ GeV/c), there are a number of drawbacks of such a system which could be improved to increase the sensitivity of the experiment. One such problem is that there would be no K/p separation at lower momenta (< 9 GeV/c). This necessarily lowers kaon tagging efficiency, since B mesons decay to protons with a rate of about 8%, and these protons, along with protons from b-baryon decay, give false flavor tags lowering kaon tagging effectiveness by 25%. No positive kaon ID below 9 GeV/c could also result in lower kaon efficiency or higher fake rate in the busy Tevatron environment. Furthermore, there are some losses of efficiency for two-body B decays like $\pi^+\pi^-$, since the tail of the pion momentum distribution extends beyond 70 GeV/c. Therefore, it will be important to extend the range of positive kaon identification down to about 3 GeV by the use of an additional device. This will not only fix the problems with K/p and K/π separation at lower momenta, but could also allow the possibility of changing the radiator to a gas with a lower index of refraction in order to shift the high end of the momentum coverage upwards to increase the efficiency for rare two-body B decays.

A cost effective solution would be to add an aerogel radiator to the gaseous RICH. Because of large Rayleigh scattering of light in aerogel, such radiators have been previously used only in threshold devices. Threshold aerogel Cherenkov counters are being constructed for the Belle experiment at KEK [4] and for the endcap region of the BaBar experiment at SLAC [5]. New production techniques developed in recent years have yielded aerogel with decreased Rayleigh scattering. While shorter wavelengths are still badly scattered, a significant fraction of visible light emerges from aerogel unscattered allowing for use in RICH detectors. Initial tests of this idea at CERN were encouraging[6]. Aerogel radiators have been proposed for RICH detectors at HERMES experiment at DESY [7] and at LHC-B [3]. However, recent preliminary results from prototype tests of the LHC-B detector at CERN indicate lower photon yield from aerogel than initially estimated [8].

At present, the largest uncertainty in the design of our PID system is related to the question about the suitability of an aerogel radiator in front of the gas radiator. To detect photons from an aerogel radiator, a larger area will have to be instrumented with photo-detectors, though with coarser segmentation. The impact of Cherenkov light from aerogel, both unscattered and scattered, on pattern recognition from photons from the gas radiator must be evaluated to ensure that high momentum PID coverage is not compromised. Finally, if an aerogel radiator turns out to be a questionable option we may want to develop some other low momentum particle identifier, for example a ToF system or DIRC.

Therefore, we would like to direct our initial R&D effort towards aerogel. Primarily we are concerned with the yield of unscattered (do we have enough photons for efficient pattern recognition ?) and scattered Cherenkov photons (source of background). The single-photon Cherenkov angle resolution from aerogel is of secondary importance, since the error is expected to be small enough that even a single photo-electron could provide 10σ K/p separation at 9 GeV/c. We need to evaluate aerogel samples from various sources. This may also involve interactions with the aerogel suppliers on production methods to minimize light scattering in visible wavelengths. A lot can be learned about aerogel properties by studying transmission of light of various wavelengths through samples of different thickness. Unscattered and scattered components can be separated by measurements at different angles. Recent other R&D efforts studied transmission only at fixed angle. Our transmission set-up would include a light source, chopper, monochromator, photo-multiplier,

movable stages to hold the radiator (radiator-on, -off for normalization) and the PM (angular dependence), a light tight box and a PC for automated measurements. The Syracuse group has experience in developing a similar system for testing the transmission of LiF and CaF_2 crystals for the CLEO-III RICH detector [9]. Results of such comprehensive transmission measurements would be used to tune our Monte Carlo program for photon propagation inside aerogel. Later, the Monte Carlo would be used to simulate Cherenkov radiation data for pattern recognition studies in a dual-radiator RICH and to produce a detailed detector design. The transmission set-up would be also used to study effects of radiation on aerogel, and to choose a material to cut-off the scattered light component. Variation in different samples of commercially available aerogel would be studied. Finally, such a set-up could be used for benchmark tests when acquiring the aerogel radiator for prototypes and the final RICH detector.

The transmission set-up would be constructed and operated by the Syracuse group. We plan to involve a postdoc, a graduate student and a technician spending 50% of their time towards this project. Skwarnicki will coordinate the RICH activity, with the other two faculty (Artuso, Stone) involved part time.

In the second year of this R&D program we would like to build a small RICH test vessel and expose an aerogel radiator to cosmic rays, and later test beam at Fermilab. To verify Cherenkov photon yields expected from the transmission measurements, a small vessel (approximate size: 1m x 0.6m x 0.6m) with proximity focussing (i.e. no mirror) would be sufficient. Such a vessel could be fit into an existing cosmic ray telescope at Syracuse which includes a pair of proportional wire chambers. Lead bricks in between the plastic trigger scintillators are used to select only relativistic muons. The telescope was previously used to test CLEO-III RICH prototypes [10]. We expect that we should be able to instrument a significant fraction of the area illuminated by Cherenkov light with photo-tubes and read-out electronics recycled from a completed Fermilab fixed target experiment (for example, Fermilab part of SELEX-RICH read-out). The other goal of this test would be to gain initial experience with multi-anode photo-tubes and HPD arrays. Therefore, a small fraction of the solid angle would be instrumented with these devices. The Syracuse group would perform these tests in collaboration with Fermilab (Linda Stutte). The Chinese groups in BTeV are interested in developing read-out electronics for RICH.

While transmission tests of aerogel samples would be brought to conclusion within the period covered by this proposal, RICH prototype work would extend beyond this period. Independent of the decision on using an aerogel radiator, a larger size prototype will need to be built with a mirror of proper radius. This will allow a study of photon yield and Cherenkov angle resolution for considered gas radiators in connection with the chosen photo-detection scheme. Cherenkov angle resolution from the aerogel radiator will also be measured in such a system. This stage of RICH R&D will be the subject of a separate, future proposal to funding agencies.

References

[1] W. Adam et al., Nucl. Inst. & Meth. **A343**, 60 (1994).

[2] J. Rosen at Workshop on Heavy Quark Physics at C-Zero, Fermilab, Dec. 4-6, 1996 and at BEAUTY '97, 5th International Workshop on B-Physics at Hadron Machines Los Angeles, 13-17 October, 1997.

[3] R. Forty, CERN-PPE/96-176, Sept. 1996 published in Proc. of the 4^{th} Int. Workshop on $B-$physics at Hadron Machines, Rome, Italy, June 1996, F. Ferroni, P. Schlein (Eds.), North-Holland, 1996.

[4] T. Iijima et al., Nucl. Inst. & Meth. **A379**, 457 (1996).

[5] D. Boutigny et al, IEEE Trans. Nucl. Sci. **44**, 1621 (1997).

[6] D.E. Field et al., Nucl. Inst. & Meth. **A349**, 431 (1994); The LHC-B Collaboration, "Status and plan of R&D for the RICH detectors of LHC-B", CERN/LHC 96-38.

[7] E. Cisbani et at, "Proposal for Dual Radiator for HERMES", HERMES-97-003, March 1997.

[8] Nick Brook at BEAUTY '97, 5th International Workshop on B-Physics at Hadron Machines Los Angeles, 13-17 October, 1997.

[9] M. Artuso at the 6^{th} International Symposium on Heavy Flavour Physics", Pisa, Italy, June 6-10, 1995; F.Constantini, M.Giorgi (Eds.), Societa Italiana di Fisica, 1996.

[10] S. Kopp, "Prototype Studies for the CLEO-III RICH", IEEE 1996, `http://suhep.phy.syr.edu/research/elementary_particles/experimental/ieee.ps`; M. Artuso et al, "Beam Tests of the CLEO-III LiF-TEA RICH Detector", `http://suhep.phy.syr.edu/research/elementary_particles/experimental/icfa.ps`.

BUDGET

Item	Cost
Transmission measurement set-up	
Lamp, chopper, monochromator	10,000
Computer controlled stages (2)	8,000
Photo-multiplier, HV supply	1,000
PC with LabView software	3,000
Light tight box	1,000
Technician (50%)	14,000
Aerogel samples	10,000
Travel (to KEK and other aerogel suppliers)	10,000
Total for transmission set-up (1st year)	57,000
Aerogel RICH prototype	
Multi-anode PMs + readout electronics	20,000
HPDs + readout electronics	20,000
Test box (materials and machining)	15,000
Travel to Fermilab	10,000
Technician (50%)	14,000
Total for aerogel RICH prototype (2nd year)	79,000

2.6 BTeV R&D Organization and Review Process

This section presents the organization of the R&D effort and outlines the procedures by which the collaboration will review and update BTeV R&D activities and milestones to reach the ultimate goals.

Each major project has a leader, or in some cases co-leaders. The major projects are:

- Simulation
- Tracking
  - Vertex Tracking
  - Forward Tracking
- Particle Identification
- Muon Detector
- Electromagnetic Calorimetry
- Trigger and Data Acquisition

It is the responsibility of each project leader to ensure the timely completion of the project milestones in a cost-effective fashion.

We expect as each of the projects begins to take shape, the project leader will create an organizational structure capable of executing the project. Because the projects vary in size, complexity, immediacy, and funding source, we plan to allow the project leader reasonable lattitude in the internal organization of the project. However, he/she must present it to the Executive Committee which must concur with the proposed structure.

2.6.1 Project Review and Goals and Milestone Tracking

A necessary feature of the R&D program is a set of reviews to ensure that the goals of the various phases of the project are achieved and to modify the plan if any step proves to be too difficult and/or costly to pursue as originally stated. For the BTEV R&D program we foresee the following review processes:

- reports by the individual R&D project leaders at each BTeV meeting (approximately every 6 weeks);
- semiannual review by the BTEV Executive Committee, arranged by the BTeV spokespersons.
- outside project reviews as deemed necessary by the BTEV Executive Committee and arranged by the BTeV spokespersons

Ultimate responsibility for the BTEV R&D plan rests with the BTEV spokespersons.

The overall progress of the R&D project is related to progress in all areas. The reports from the project leaders at the BTEV Collaboration meeting will identify areas of conflict or schedule difficulties and allow the BTeV leadership to respond. From these reports, perhaps with additional material submitted for backup, we will create the ongoing record of the project and any specific reports required by Fermilab and the relevant funding agencies to permit them to accomplish their management and oversight roles.

i. Semiannual Review by BTEV Executive Committee

The milestones for the BTeV R&D project are spread over a 3 year period. In addition to the regular reports at the Collaboration meeting, an in-depth review of progress and problems should be organized twice a year. The review will be organized by the BTeV spokespersons who may, if they choose, bring in outside experts to aid in the review.

ii. Outside Project Reviews

If the situation warrants, an extensive outside review of the whole R&D project or any part of it can be organized by the BTEV spokespersons, with the concurrence of the Executive Committee.

iii. Formal Project Management

The experiment is committed to adopting a formal project management structure and plans to work with Fermilab and other funding agnecies to establish the appropriate framework from the outset of the project.

2.6.2 Collaboration with External Organizations

Collaboration with industry, academic institutions, and other laboratories and experiments is viewed as essential to achieving BTeV goals in a timely and cost-effective manner. The individual project leaders, with the concurrence of the Executive Committee, may enter collaborative agreements.

We have already started several collaborative efforts with external institutions and industries to take full advantage of the experience and the technologies in maturing fields.

The collaborations we have established so far, which are all in the area of pixel R&D, are the following:

- Brookhaven National Lab and John Hopkins University on sensor development;
- LBNL and Boeing North America, Inc. on bump bonding;
- The CERN RD42 Collaboration on research and development of diamond pixel detectors; and
- The ATLAS collaboration on sensors and staggered layout.

We are also in close contact with other institutions working on pixel systems for LHC experiments(CMS and ALICE) and additional collaborative arrangements are likely to be made soon.

A Summary of Pixel R&D at Fermilab

A.1 Introduction

At the start of 1997, Fermilab formed a Pixel R&D group which coordinates the R&D on pixel detectors for all the Tevatron experiments, including BTeV. Several members of the group are also members of the BTeV collaboration. Many activities of the group are joint efforts with the Electronic Systems Engineering (ESE) Dept. in the Computing Division and the Electrical Support Team and Microdetector R&D group of the Silicon Detector Facility of the Particle Physics Division (PPD) of Fermilab. In this brief report, we summarize the results that have been achieved recently.

Our main accomplishment for FY97 was to gain first hand experience in putting a hybridized pixel detector (silicon pixel sensor array bump bonded to a readout chip) together and operating it. By this, we mean that we have gone through all the steps in the design, fabrication and testing of a small pixel detector. We have also prepared infrastructure (including a silicon strip detector telescope) for beam tests, and established working relationships with the above groups (helping define and develop their ability to support our present and future efforts) as well as outside groups working on pixel detectors and radiation-hardened silicon sensors. Contacts have also been made with various companies and institutes specialized in bump-bonding, chip repair, mask fabrication and silicon foundries.

A pixel analog front-end chip has been acquired (from a SLAC CRADA) and tested at Fermilab. Preliminary results on the chip will be presented in Section A.3. We have also designed and received some detector wafers fabricated at BNL which have pixel sensors matching the front-end chip. The design and fabrication process has been presented recently at the IEEE NSS in Albuquerque. To mate the two together, we have worked with two vendors. Hybridized detectors have been delivered from both vendors and are now being tested and evaluated.

At the same time, the ASIC group in the Electrical Support Team has designed and fabricated a pixel readout chip. Tests are currently being carried out on this chip. Preliminary results will be presented in Section A.4. Test results on both chips have been presented recently at the Front-End Electronics Workshop at Taos. Two rad-hard pixel detector test structures were designed and (with help from the Electrical Support Team) laid out. These test detectors are being fabricated by CiS (in Germany) and SII (Seiko Instruments Inc.,Japan) as part of the ATLAS pixel submission. Detectors are also being produced by ICM (in the Czech Republic). The detectors are intended to test an idea for coupling fine pitch detector pixels to wider pitch electronics pixels (staggered geometry). If successful, this idea might significantly reduce the technical risk and hence the cost of fine-pitch bump-bonded pixel detectors. The detectors are also intended to yield information on the finest pitch which is achievable with a (rad-hard) n+ on n silicon pixel detector. Delivery of these test devices is expected early in 1998.

A.2 Readout Chip

Two readout chips have been tested: the data-push AIC501 chip (from the SLAC CRADA) and the first generation Fermilab pixel readout chip FPIX0. Tables 10 and 11 summarize the main design parameters and the preliminary measurements. There are major differences (operational, functional, size etc) between the two chips so that a direct comparison of the performance of the two just by inference from the tables is inappropriate.

The AIC501 chip has a column-row architecture and has minimal digital function. By working with an existing chip, we were able to get first hand experience in the assembly, operation, and testing of a pixel detector. This allowed us relatively quickly to get into key issues on development of sensor to be mated to the chip, bump bonding, and detector assembly.

The FPIX0 chip is the first product of an ambitious program which demonstrates that we have the capability in-house to take on pixel readout chip design and development. The chip already has a lot of functionality (eg. End of Column logic) which can be scaled up directly to a full-size chip. Both analog front end and the digital periphery are integrated on the same chip and this design allows us to study cross-talk,

and the effect of digital noise on the front-end. The chip was designed, fabricated and tested within a few months period. As can be seen from Table 11, most of the design goals have been met or exceeded.

A.3 Preliminary Results on the Data-push AIC501 chip

The development of the data push architecture (DPA) for a pixel readout chip dates back to the SSC days. It was motivated by two goals: the first, having a simple, rugged, small chip periphery, resulting in minimal dead area, and the second, the desire to have the silicon vertex detector participate in the trigger.

The data push architecture allows the detection of the incident particle to initiate the read sequence, sending the address of the "hit" in terms of rows and columns within the pixel array, the time of arrival, and the pulse height reflecting the energy deposited by the detected particle onto a data bus for use by the trigger system. Another significant feature of the design was the specification that the maximum time necessary to completely read out one "hit" (designed as the pixel having the largest signal and its two adjacent neighbors within the same column) would be less than 200ns. To achieve this throughput specification, the pixel's digital periphery employs sparse scanning, self clocking and priority selection.

With the cancellation of the SSC, the SLAC group continued the effort with some funding from a CRADA whose goal was the development of a pixel detector for X-ray diagnostic use. The chip was fabricated using HP 1.2 micron CMOS process. Each chip is a 16x16 array, with a pixel size of 30x200 microns square. The cell contains only analog front-end circuitry. Due to the lack of funding, the digital companion to the analog chip was not fabricated.

A.3.1 Test Results

We have obtained from the SLAC group (courtesy of S. Shapiro who is now a BTeV collaborator) the DPA chips (AIC501). Together with the ESE department, we have done some measurements on the bare chips. All the control and digital part of the circuitry was done by using discrete components assembled in a custom made PC board. The measurements were done in a noisy environment so these numbers should be taken as preliminary.

General Characteristics

The digital periphery of the AIC501 chip is designed to transmit only bone-fide hits, no zero's and no ghosts. This design eliminates a number of problems inherent in previous designs. The effects of threshold mismatches and nonuniformities have been reduced by the use of sampled data techniques to reset the pixel comparator. The use of a destructive readout rather than storing the pulse height for later retrieval reduces the parts count within the pixel and insures its integrity. Crosstalk due to large voltage swings on traces which abut adjacent pixels has been virtually eliminated by the use of current mode output drivers. Finally, chip dead time has been reduced to a minimum by the infrequent need to reset the front-end amplifier when the leakage current from the sensor array is negligible.

Parameter	*Design Goal*	*Measured*
$TimeWalk[4-50Ke^-]$	$< 250\ ns$	$15\ ns$
Noise	$< 200\ e^-$ rms	$< 130\ e^-$ rms
Gain Uniformity	3%	$< 3\%$
Threshold Sensitivity	$1K - 4K\ e^-$	$1.3K - 5K\ e^-$
Threshold Uniformity	3%	2.65%
Power Consumption	$< 30\ \mu W$	–
Input Dynamic Range	$> 45K\ e^-$	$45K\ e^-$
Pixel Comparator Reset	$< 200\ ns$	$180ns$
Chip Reset	$< 1000\ ns$	$240ns$

Table 10: Summary of the design specifications and the preliminary measured parameters for the AIC501 chip.

The input amplifier is a single stage cascoded inverting amplifier followed by a buffer stage. The feedback capacitor is designed to be 10fF, corresponding to 16 μV per electron. Thus, a minimum ionizing particle passing through 300 μm of silicon produces about 0.4V at the preamp output.

The operating cycle of the chip begins with the pixel comparator firing on the detection of a signal (from a particle or test input). It generates a current and sends it to the current-to-voltage converter (I-V) at the column periphery. The I-V causes a HIT signal to be generated by the digital logic which records the time and column address of the hit, and resets all of the comparators which have been fired. The digital and analog information is stored in the pixel at this time, The control logic then issues a Digital Read command to the entire hit column highest on the column priority encoder list. The pattern on the ROWOUT lines is stored as the row address information, and an Analog Read signal issued, one at a time, to each row with data.

Table 10 summarizes the main parameters of the front-end analog design.

Time Walk

Time walk refers to the fact that the comparator in the unit cell gives an output which is more delayed for small signals than for large ones. The effect of time walk is felt most for particles which cross multiple columns. For the present measurement, we define time walk as the difference in this delay time for signals twice the threshold as compared to very large signals. Our preliminary measurements for the DPA501 chip gave a time walk of 15 ns at a threshold of 2K electrons with a dispersion error of 1.6 ns. Fig. 25 shows the preliminary measurements of the time delay at two different threshold settings.

Noise

We measure the noise generated by the preamp in the bare chip. Due to the noisy environment in which the tests were being done, the measurements reported here should be regarded as the upper limit. The fitted mean of the noise distribution from about 200 cells is 132 electrons with a σ of 16 electrons. The distribution is random with no sign of correlation between any particular row or columns. Fig. 26 shows the noise distribution.

Gain

The dynamic range should be able to handle the charge deposited by a minimum ionizing particle traversing 300 μm of silicon (25K electron-hole pairs). Large incident angles, Landau fluctuations, delta rays as well as more than one minimum ionizing particle traversing the same pixel will provide a larger charge signal. On the other hand, to deal with small signals (eg. thin detectors or detector after irradiation) and the high degree of charge sharing anticipated in a forward B-spectrometer, the low end of the dynamic range has to be set to 1K e^- or less. The circuit should record with high linearity the charge deposited up to a signal of about 50K electrons in order for its pulse height information to be useful. Another important parameter is the uniformity of gain in the chip. Any large gain variation uncorrected for in the readout chip would result in inaccurate measurement of the charge sharing necessary for the high spatial resolution. For the present chip, the gain variation has been measured to be under 5% at the largest input signal (40Ke^-).

Threshold for pixel comparator

The threshold for the pixel comparator is envisioned to be set at ten times the noise specification in order to keep the spurious hit rate at a very low value. It is important that the thresholds for different pixels in a chip be reasonably uniform. For the present chip, the threshold uniformity has been found to be very good, ranging within a few percent of the average value when the average value is set to 3K electrons. The threshold distribution is shown in Fig. 27.

Parameter	*Design Goal*	*Nominal*	*VLCf*
Time Walk$[4-50Ke^-]$	65 *ns*	18 *ns*	18 *ns*
Noise	100 e^- *rms*	57 e^- rms	38 e^- *rms*
Cross Talk	$< 5\%$(*detector*)	$< 0.2\%$(*chip*)	$< 0.4\%$(*chip*)
Threshold Sensitivity	$2.5K$	$0.7K$	$0.5K$
Threshold Uniformity	$1K$ $e^-(p-p)$	168 $e^-(rms)$	100 $e^-(rms)$
Power Consumption	< 50 μW	36 μW	36 μW

Table 11: Summary of the design specifications and the measured parameters for the FPIX0 chip.

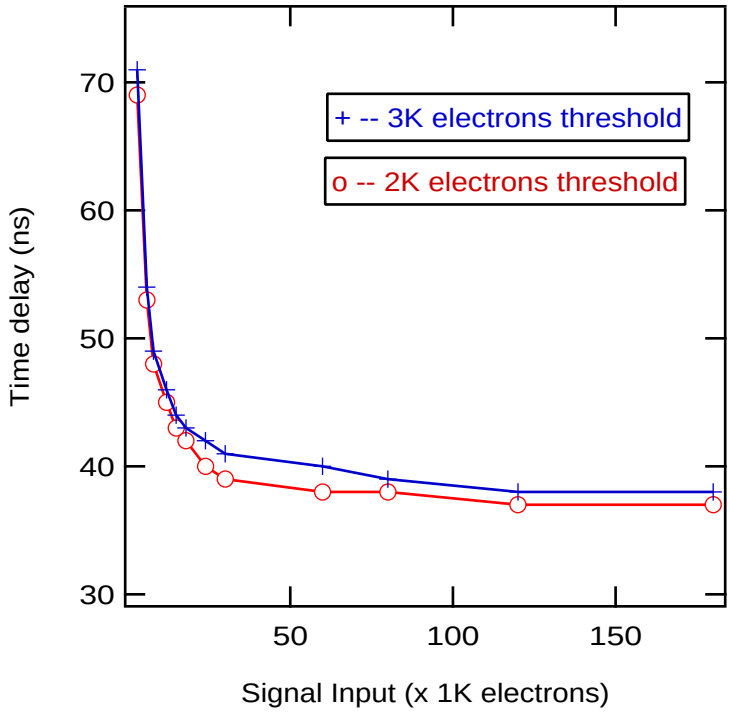

Figure 25: Time delay curve for the AIC501 chip at two different threshold settings.

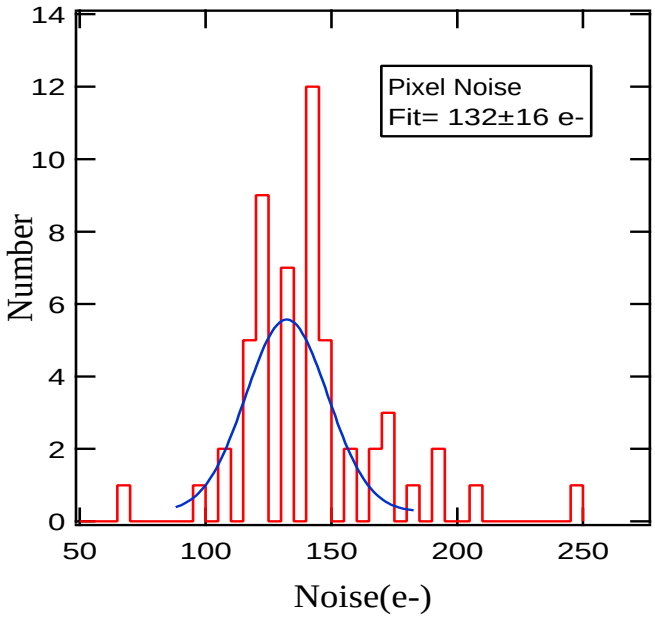

Figure 26: Noise distribution from different pixels on the AIC501 chip

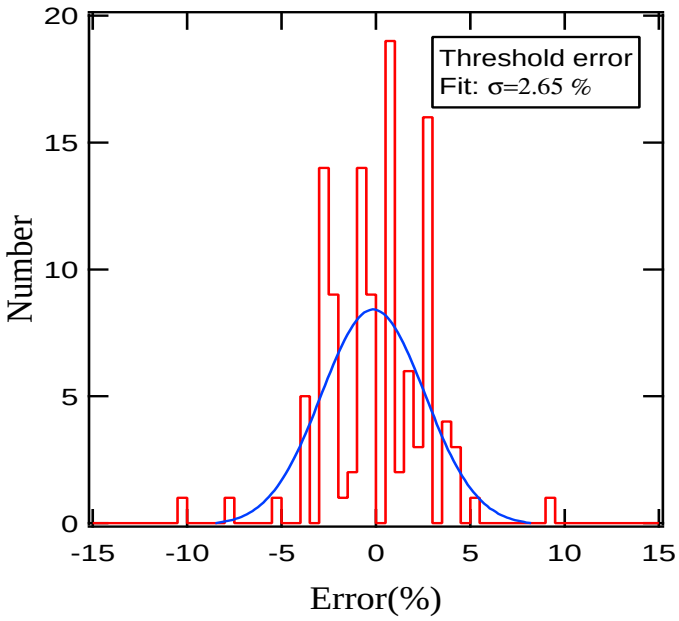

Figure 27: Threshold distribution from different pixels on the AIC501 chip.

Cross-talk
We have measured two different chips and observed no cross-talk in either at different threshold settings (1.6K to 4K electrons) even when a large charge signal is injected in a neighboring cell.

A.4 Preliminary Results on the FPIX0 chip

The ASIC group at Fermilab has designed a first generation readout chip which is tailored to the 132ns bunch crossing at the Tevatron. The objectives are to:

1. establish a baseline solution for the analog Front End
2. learn and acquire experience needed to build a complex pixel detector

The circuit has a two stage configuration with the stages AC coupled. The second stage is DC coupled to the discriminator, which is a two stage comparator. The first stage is a charge amplifier that uses a variant of the current controlled active feedback circuit that CPPM (Marseille) has developed for ATLAS. The feedback current controls the return to baseline time and leakage compensation. The threshold of the comparator is independent of the leakage induced DC shift in the preamp. Thus, this design will in principle, be immune to the effect of high leakage current from the sensor after irradiation. The cell logic is simple. It stores the hit in a flip-flop, asserts a Fast OR and waits for a token. Upon receipt of a token, it generates a GETBUS signal that enables the address switches to take the global bus and a Sample/GBUS signal for the Peak Sensing Circuit to take the global analog-out line. When a TOKEN-ADV signal is received, the cell clears itself and the peak circuit, passes the token to the next hit pixel(if any). The End of Column (EOC) logic stores the content of the Beam Crossing (BCO) counter in the BCO register and disables the column until readout.

The chip is a 12x64 array, with each pixel being 50x400 microns. This dimension is chosen such that it can be bump-bonded to sensor arrays obtained readily from the ATLAS collaboration. The cell is of two types - a "nominal" one and a special one called VLCf which has a lower feedback cap (higher gain) and lower noise, but higher crosstalk. The digital and analog output of the whole top row of the chip is buffered and available for tests and diagnostics. The chip is fabricated in HP 0.8 micron CMOS process. All the measurements were done under the same nominal conditions (3V and 36 μW/cell) and an automatic scanning of the whole

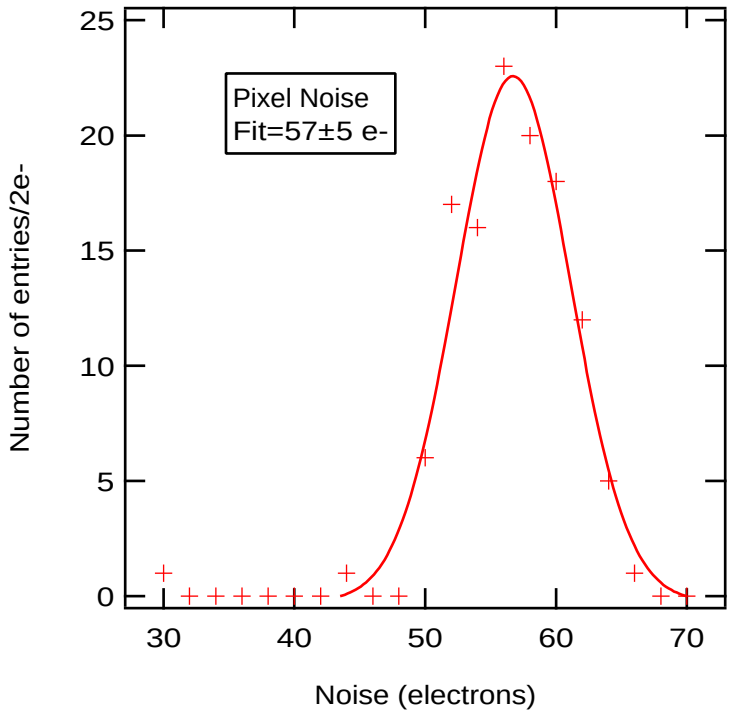

Figure 28: Noise distribution of the nominal cells in the FPIX0 chip.

array was performed. After the tests were done, it was found that the chip was exposed during the tests to some ambient light and the noise measurements were repeated with a better light shield.

A.4.1 Preliminary Results

Noise
With nominal setting, the noise has been inferred as 57 e^- rms for the nominal cell and 38e^- for the VLCf cell. The noise variation from cell to cell is distributed randomly in the chip (independent of the location of the cell). Fig. 28 shows the noise distribution for a large number of nominal cells in a single chip.

Time Walk
Fig. 29 shows the time delay curves for a nominal cell at a threshold setting of 2.5K electrons. There is little variation between different cells.

Threshold
The minimum threshold was 708 e^- (nominal cell) and 500e^- (for VLCf), with a spread of 168 e^- (nominal) and 100 e^- (VLCf). This spread was found to be independent of the threshold setting. There are two bias currents and one threshold control. Threshold and noise extraction was determined by two methods: the Sigmoid fit and the Linear Fit. The threshold variation is, to first order, independent of the threshold setting, location of the cell, particular row or column. Fig. 30 shows the threshold distribution for the nominal cells.

Gain Linearity
For an input signal of $< 16Ke^-$, the linearity of the amplifier has been measured to be $< 0.6\%$. When the input signal is increased to $< 25Ke^-$, the corresponding number for linearity is $< 3.5\%$. The preamp is linear up to about $20Ke^-$ and then it saturates. Gain variation across the chip has been measured to be about 8%.

Readout Speed
Readout speed is about 156 ns for 3 contiguous hit pixels (in the same column) for binary readout only.

General Characteristics
The nominal rise time of the front end and buffer has been measured to be 40 ns and the pixel recovery time to be 545 ns. These timing numbers, particularly the latter one, can be adjusted over a wide range

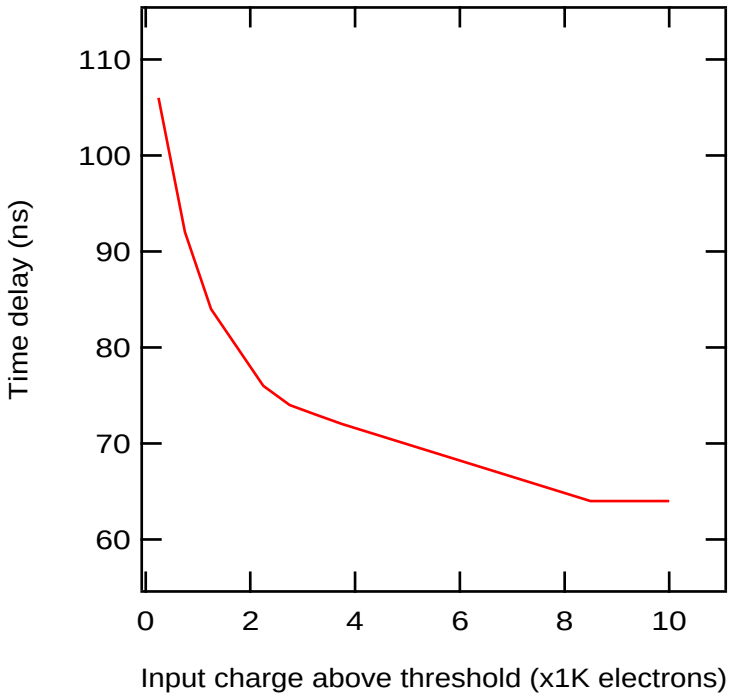

Figure 29: Time delay curve for the FPIX0 chip at a threshold setting of 2.5K electrons.

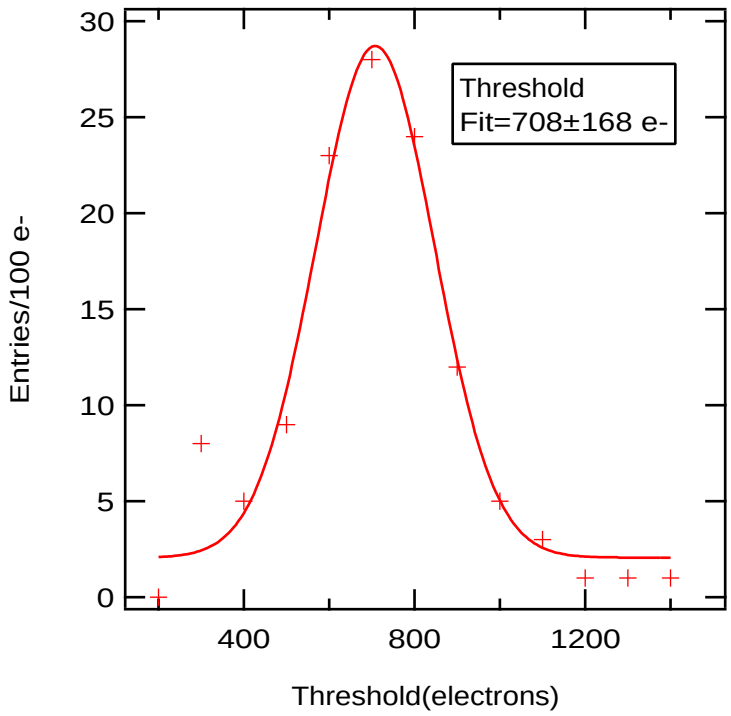

Figure 30: Threshold distribution for the FPIX0 chip.

depending on the settings. Other features of the chip include individual injection of test signals, killing of noisy pixels, and a peak-sensing detector which works to 4-5 ADC bit precision. So far, two chips have been measured and all the characteristics are in good agreement between the two. All the tests presented here need to be confirmed by changing the test conditions (say 4V bias). Also, the results are from the bare chip. To fully understand and debug the chip, one needs to bump-bond it to a detector.

A.5 Sensor Array

In the BTeV basline pixel system, each quadrant is placed as close as ±6mm from the colliding beam. This poses severe radiation level for the innermost region of the pixel system. At the highest luminosity (2 x 10^{32}), type inversion may occur after several months of operation and the silicon pixel sensors have to be operated at very high bias (hundreds of volts) to obtain full depletion. These requirements demand new directions in detector design and material selection. Since the problem is the same for the LHC experiments, we can benefit from experiences of other groups. Some members of the Fermilab Pixel R&D group have joined the CERN RD48 collaboration (R&D on Silicon for future experiments) to work on the problems of bulk damage in silicon resulting from irradiation.

We are also working together with Brookhaven National Laboratory and Johns Hopkins University in designing, fabricating (at BNL) and testing of pixel detectors before and after irradiation. Multi guard-rings structures are designed for high voltage (up to 400 volts) operation and are currently being evaluated. Material characteristics, chosen to increase hardness are also studied. These include low resistivity (1.9 KΩ-cm) n-type silicon wafers (this will delay the occurrence of type inversion) and thinned wafers (down to 200 μm) to reduce full depletion voltage. Both p+/n/n+ and n+/n/p+ pixel detectors of various configurations have been fabricated at BNL.

For the sensors that are used for the construction of the hybridized detector, we follow two paths, one for each of the chips that we are testing. For the AIC501 chip, we use high resistivity (4-6KΩ-cm)n-type silicon wafers of 4 inch in diameter and 300 microns in thickness. These are p+ pixels on n-bulk detectors and are fabricated at BNL. Four wafers have been delivered.

The FPIX0 chip has been designed with the idea of obtaining matching pixel sensor arrays from the ATLAS collaboration. As mentioned before, sensors arrays which match these readout chips can be obtained from the ATLAS submission and we have some tentative agreement with them to obtain a few arrays for our studies. We will also obtain a few wafers of detectors from ICM (formerly Tesla, in the Czech Republic).

A.6 Bump Bonding

The BTeV baseline pixel detector, like all other pixel systems, is based on a design relying on a hybrid approach. With this approach, the readout chip and the sensor array could be developed separately and the detector is constructed by flip-chip mating of the two together. This method offers maximum flexibility in the development process. choice of fabrication technologies, and the choice of sensor materials. However, it requires the availability of a highly reliable, reasonably low cost fine-pitch flip-chip attachment technology.

There are several bonding technologies which may be suitable for this. These include Indium bumps, Pb-Sn solder bumps, fluxless solder bumps and anisotropic conductive films (ACF) or tapes. Table 12 lists the different vendors that we have approached and their capabilities.

Given the fact that we are dealing with dies at this phase, and that our pitch is extremely fine, we chose to go with In bumps which possess many attractive features. Indium bumps have been grown on 30 micron pitch for an earlier beam tests of an hybridized array in the 1991 Fermilab fixed target run. The low melting point of pure indium, 156 deg C, allows for cold pressure welding instead of solder reflow and low forces (2-3 gram/bump) are used during the bonding process. For small prototype runs, there are only a handful of companies that can provide such services to outside customers. Given the technical challenges (small die, large aspect ratio, fine pitch), we decided to go to two different vendors. These are Advanced Interconnect Technology (AIT), a San Jose based company with a production facility in Hong Kong and Boeing North America Inc. in Anaheim. Indium bumps of under 16 microns in diameter which have been successfully deposited on our detector arrays by Boeing. We have already received four hybridized detectors each from AIT and BOEING and these detectors will be evaluated soon.

Vendor	*Technology*	*Min. pitch*	*Min. diam.*	*Mating*	*Die*
Boeing	*In(dep.)*	$40\mu m$	$15\mu m$	*yes*	*yes*
Cincinnati	*In(dep.)*	$50\mu m$	$15\mu m$	*yes*	*limited*
AIT	*In(dep.)*	$40\mu m$	$12\mu m$	*yes*	*yes*
	solder	$150\mu m$	$100\mu m$	*yes*	*no*
SII	*solder*	$50\mu m$	$25\mu m$	*partial*	*no*
	ACF	$100\mu m$		*yes*	*no*
DTO	*In(elect.)*	$50\mu m$	$25\mu m$	*no*	*no*
	solder	$50\mu m$	$30\mu m$	*no*	*no*
MCNC	*solder*	$75\mu m$	$25\mu m$	*yes*	*no*
	fluxless solder	$125\mu m$	$30\mu m$	*yes*	*no*

Table 12: A list of vendors that can provide bump-bonding services. Dep. means that the bumps are vacuum deposited. Elect. means electroplating.